



저작자표시-비영리-변경금지 2.0 대한민국

이용자는 아래의 조건을 따르는 경우에 한하여 자유롭게

- 이 저작물을 복제, 배포, 전송, 전시, 공연 및 방송할 수 있습니다.

다음과 같은 조건을 따라야 합니다:



저작자표시. 귀하는 원저작자를 표시하여야 합니다.



비영리. 귀하는 이 저작물을 영리 목적으로 이용할 수 없습니다.



변경금지. 귀하는 이 저작물을 개작, 변형 또는 가공할 수 없습니다.

- 귀하는, 이 저작물의 재이용이나 배포의 경우, 이 저작물에 적용된 이용허락조건을 명확하게 나타내어야 합니다.
- 저작권자로부터 별도의 허가를 받으면 이러한 조건들은 적용되지 않습니다.

저작권법에 따른 이용자의 권리는 위의 내용에 의하여 영향을 받지 않습니다.

이것은 [이용허락규약\(Legal Code\)](#)을 이해하기 쉽게 요약한 것입니다.

[Disclaimer](#)

Master of Science

Robust Position and Vibration Control of An Electrohydraulic Series

Elastic Manipulator against Disturbance Generated by A Variable

Stiffness Actuator

The Graduate School of the University of Ulsan

Department of Mechanical Engineering

NGUYEN MINH NHAT

Robust Position and Vibration Control of An Electrohydraulic Series
Elastic Manipulator against Disturbance Generated by

A Variable Stiffness Actuator

Supervisor: Prof. Kyoung Kwan Ahn

A Dissertation Submitted to

The Graduate School of the University of Ulsan

In Partial Fulfillment of the Requirements

For the Degree of Master of Science

By

NGUYEN MINH NHAT

Department of Mechanical Engineering

Ulsan, Korea

December, 2017

기계자동차공학과


**ROBUST VIBRATION AND POSITION CONTROL OF AN
ELECTROHYDRAULIC SERIES ELASTIC MANIPULATOR
UNDER DISTURBANCE BY THE VARIABLE STIFFNESS
ACTUATOR**

This certifies that the dissertation of

NGUYEN MINH NHAT is approved by:

Committee Chairman:

Prof. BYUNG RYONG LEE



Committee Member:

Prof. SOON YONG YANG



Committee Member:

Prof. KYOUNG KWAN AHN



School of Mechanical and Automotive Engineering

University of Ulsan, Korea

October, 2017

Acknowledgments

First and foremost, I wish to express my sense of gratitude and indebtedness to my supervisor Prof. Ahn Kyoung Kwan for his inspiring guidance, encouragement, and untiring efforts throughout my study in University of Ulsan. All my theoretical design, fabrication, hardware, and control system for this study could not be employed without his help.

I also would like to thank professors in the committee, Prof. Yang Soon Young, Prof. Lee Byung Ryoung and Prof. Ahn Kyoung Kwan, for their comments and suggestions throughout this study.

Finally, I would like to thank especially my family, my Cuc No, Mr Tran Duc Thien, all my brotherhoods in FPMI Lab for their encouragement, understanding as well as friendship.

Contents

Acknowledgements	I
Contents	II
List of Figures.....	IV
List of Tables	VI
Nomenclature	VII
ABSTRACT	VIII
Chapter 1. INTRODUCTION	1
1.1 Overview	1
1.2 Research objective.....	3
1.3 Outline of the thesis.....	4
Chapter 2. PROPOSED ELECTROHYDRAULIC SERIES ELASTIC MANIPULATOR SYSTEM WITH A NOVEL VARIABLE STIFFNESS ACTUATOR	5
2.1 Background of a hydraulic system	5
2.1.1 Characteristics of hydraulic systems.....	5
2.1.2 Applicability of hydraulic systems	5
2.2 Electrohydraulic servo system.....	6
2.3 Series elastic manipulator with a novel variable stiffness actuator	7
2.3.1 Background of variable stiffness actuator.....	7
2.3.2 Proposed variable stiffness actuator for series elastic manipulator.....	9
2.4 System mathematical modeling.....	11
2.4.1 Model of electrohydraulic servo valve system.....	11
2.4.2 Model of variable stiffness actuator	12
2.4.3 Model of series elastic manipulator	13
Chapter 3. CONTROL DESIGN.....	19
3.1 Overview of the hybrid controller	19
3.2 Design of Adaptive Input Shaping	19
3.2.1 Conventional Input Shaper - ZV and ZVD.....	19
3.2.2 Proposed Adaptive Input Shaping	23
3.3 Design of Backstepping Adaptive Enhanced Fuzzy Sliding Mode controller.....	24

Chapter 4. EXPERIMENTAL RESULTS	32
4.1 Testbench setup.....	32
4.2 The variation performance of the VSA system	35
4.3 Case study 1	35
4.4 Case study 2	37
4.5 Case study 3	39
4.6 Case study 4	41
Chapter 5. CONCLUSIONS AND FUTURE WORKS	46
References	48

List of Figures

Figure 1 VSA in a rotational joint	2
Figure 2 VSA in a hopping robot.....	2
Figure 3 The bidirectional antagonistic	2
Figure 4 Structure of the electrohydraulic servo system.....	6
Figure 5 Manipulator with programmable passive impedance	7
Figure 6 McKibben artificial muscle	7
Figure 7 DLR light-weight robot.....	8
Figure 8 Proposed variable stiffness actuator	11
Figure 9 VSA forces analysis	12
Figure 10 System parameters assignment.....	15
Figure 11 Structure of the hybrid controller	19
Figure 12 Two impulse response	20
Figure 13 Continuous shaper input.....	22
Figure 14 Sensitivity curves	22
Figure 15 MFs for input/output of the proposed FIS.....	24
Figure 16 Membership functions of fuzzy sets for EFSMC of outer loop.....	25
Figure 17 Membership functions of fuzzy sets for EFSMC of inner loop.....	29
Figure 18 Scheme of BPID controller for the ESEM system	30
Figure 19 Scheme of BSMC controller for the ESEM system	31
Figure 20 Schematic diagram of the electrohydraulic-series-elastic-manipulator system.....	32
Figure 21 The experimental apparatus.....	34
Figure 22 Bode plot of the VSA system with a PID controller	35
Figure 23 Comparison of the sinusoidal response of the ESEM system.	36
Figure 24 Comparison of the sinusoidal torque response of the ESEM system. a) PID b) BSMC c) BAEFSMC	36
Figure 25 Comparison of the sinusoidal control signal. a) PID b) BSMC c) BAEFSMC	37
Figure 26 Comparison of the pulse position response of the ESEM system.	38

Figure 27 Comparison of the pulse torque response of the ESEM system. a) PID b) BSMC c) BAEFSMC	38
Figure 28 Comparison of the pulse control signal. a) PID b) BSMC c) BAEFSMC	39
Figure 29 Comparison of the multi-step position response of the ESEM system.....	40
Figure 30 Comparison of the multi-step torque response of the ESEM system. a) PID b) BSMC c) BAEFSMC	40
Figure 31 Comparison of the multi-step control signal. a) PID b) BSMC c) BAEFSMC	41
Figure 32 The periodogram of the end effector oscillation	42
Figure 33 Vibration response of the end effector with ZV	43
Figure 34 Vibration response of the end effector with ZVD	43
Figure 35 The vibration response of the end effector with FIS	44
Figure 36 The adaptive parameters of the FIS	44
Figure 37 The vibration response at two positions of the VSA	45
Figure 38 Position response of the ESEM system with BAEFSMC and FIS	45

List of Tables

Table 1 Characteristics comparison of VSA systems	9
Table 2 Link parameters of the two-link planar manipulator	14
Table 3 Rule table of the fuzzy inference	23
Table 4 Setting parameters for the ESEM system	32

Nomenclature

ESEM	Electrohydraulic Series Elastic Manipulator
VSA	Variable Stiffness Actuator
EHS	Electro-Hydraulic Servo
SEM	Series Elastic Manipulator
AEFSMC	Adaptive Enhanced Fuzzy Sliding Mode Control
DOF	Degree of Freedom
IST	Input Shaping Technique
AIS	Adaptive Input Shaping
IS	Input Shaping
PID	Proportional Integral Derivative
SMC	Sliding Mode Control
FIS	Fuzzy Input Shaping
BAEFSMC	Backstepping Adaptive Enhanced Fuzzy Sliding Mode Control
LWRs	Light Weight Robot system
ASBM	Adjustable Spring Base Mechanism
BPID	Backstepping Proportional Integral Derivative
BSMC	Backstepping Sliding Mode Control
ZV	Zero Vibration
ZVD	Zero Vibration Derivative

Abstract

Traditionally, robots are used to handle the repetitive tasks precisely in complex environments. They are normally characterized by rigid links and powerful actuators, making them dangerous for human workers. Thus, to improve the workplace safety, robots-human interaction trends to become one of the most interest topics. The arm is paid for the flexible impedance properties, such as adjusting the robot equilibrium, the stiffness, and the damping. Variable stiffness concepts were developed to reach a compromise of accuracy execution and safe operation.

This thesis proposes an electrohydraulic series elastic manipulator (ESEM) with a novel variable stiffness actuator (VSA). As the results, the combination provides a number of advantages such as highly efficient in transmitting power, less maintenance requirement, high dynamic and wide range of stiffness adjustment. However, the nonlinear behaviors and modeling uncertainties such as, friction, internal and external leakage of the electrohydraulic servo (EHS) system as well as the complex model of the series elastic manipulator (SEM) system are major challenges for the precise position control. In addition, the spring connection of the manipulator causes the vibration at the end effector during the trajectory tracking.

In other to eliminate the oscillation of the end effector, a new vibration control method is proposed based on the characteristics of the ESEM system to suppress the residual vibration robustly to the stiffness regulation. The trajectory tracking controller utilizing backstepping technique is divided into two loops, based on system states, the position control loop and the torque control loop. An adaptive enhanced fuzzy sliding mode control (AEFSMC) was applied for each loop to ensure the stability and the robustness in the presence of the known uncertainty of both mechanical and hydraulic system such as friction, leakages, disturbance torques. The stability of the overall closed-loop system was proven by Lyapunov's theory.

By a number of real-time experiments, the effectiveness of the hybrid controller was proved via the stability and accuracy in position and vibration control of the ESEM system under disturbance by using the VSA system.

INTRODUCTION

1.1 Overview

Variable stiffness actuators (VSA) can improve the robot's performance during interactions with human and uncertain environments. Several prototypes of single-degree-of-freedom (DOF) joints containing the adjustable compliance for robotic manipulators have been designed and developed [1-7]. Figure 1 to Figure 3 show some application of the VSA system in practical systems. These studies used DC motor which is normally low torque/force to weight ratio as the actuators. The series connection of those actuators also causes couple torques on each other and stiffness regulation in a short range. This paper proposes a robotic manipulator using the electrohydraulic servo (EHS) system as the primary torque generator. To realize the stiffness adjustment, another mechanism which is based on the combination of a SEM and an adjustable spring base to change the position and the acting forces of the springs. Because of the springs connection between two links, the oscillation at the end effector will occur during the trajectory tracking of the manipulator. Input shaping technique (IST), a feed-forward scheme was introduced by Singer and Seering [8] to eliminate the system residual vibration. IST has been used in practical systems such as flexible manipulator [9], ship cranes [10]. However, IST is not able to apply for the ESEM system containing the VSA system which has a wide range of oscillation parameter variations. To overcome this disadvantage, there were several adaptive input shaping (AIS) schemes have been developed. E. Pereira et al. [11] used the algebraic identification method to obtain the natural frequency of the arm. J. Park et al. [12] proposed the learning input shaping technique to update the IS parameters based on magnitude and phase difference of residual vibration. However, these schemes require the detail dynamic model of the plant or need several cycles to turn the adaptive values.

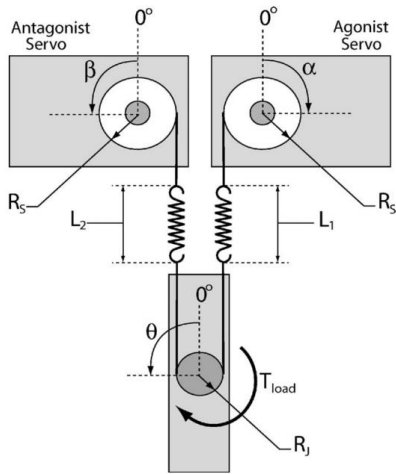


Figure 1 VSA in a rotational joint

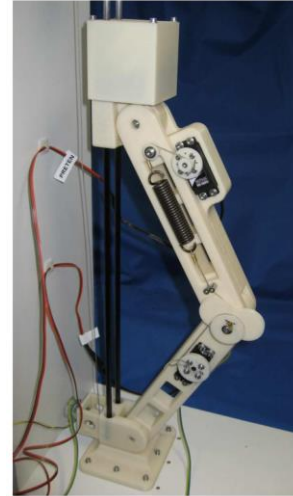


Figure 2 VSA in a hopping robot

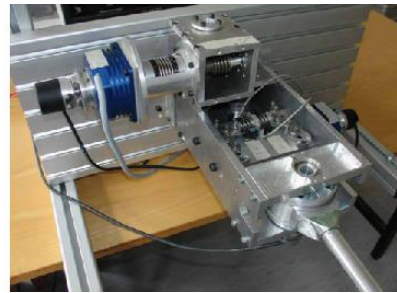
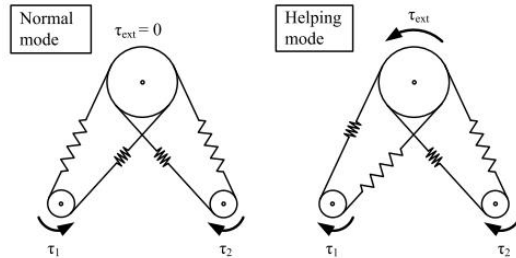


Figure 3 The bidirectional antagonistic

The ESEM includes an electrohydraulic actuator for the equilibrium position and springs with the electric motor for the adjustable stiffness mechanism, so the complete nonlinear dynamic equations shows that the ESEM is a highly nonlinear system. These elements are a major obstacle for the control designing. Various control methods have been used for trajectory tracking control of hydraulic cylinder. The PID controllers [13] [14] [15] were investigated to control the position and force tracking for the electro-hydraulic actuator (EHA). The feedback linearization was used in some research works [16], but these methods did not account for the nonlinear dynamics of the cylinder and uncertain fluid parameters. Therefore, several kinds of sliding mode control (SMC) methods are adopted for the EHS system [17] [18]. However, the SMC requires the knowledge of uncertainty bound which is difficult to obtain in a practical system. The chattering phenomenon is also a disadvantage in practical applying of the SMC [19]. Thus, adaptive control has been proposed to deal with above problems, sliding mode adaptive control [20] [21], feedback linearization adaptive control [22]. Although these nonlinear control schemes showed the chattering elimination; good tracking performance; and robust to uncertainties, the considered controlled plant appears to be a hydraulic actuator

which has a simpler mathematical model than the ESEM system. Besides, the actuator dynamics in these systems are typically excluded from the system behavior to simplify the control design. The control scheme has been employed without considering the actuator dynamics, and it includes proportional control for position control and SMC for speed control. In this ESEM system, the actuator dynamics are very complicated, especially due to the high nonlinearities of the valve dynamic and leakages. They can influence the dynamic characteristics and stability.

1.2 Research Objective

Based on the above analysis, an electrohydraulic series elastic manipulator (ESEM) containing a novel variable stiffness actuator (VSA) is proposed and discussed. The ESEM system can be used efficiently for lift assist or industrial manipulators to increase workplace safety for human workers as well as provide suitable dynamics in unknown and dynamic environments [23]. Shocks can be absorbed by springs to prevent damage to the transmission of the actuator, which improves the safety of the robots. The lower reflected inertia can provide safe interaction with humans. The springs can also exchange energy with the environment to reduce the energy consumption in work requiring a high burst of power (such as the VIA joint prototype [24], a soccer-ball kicking leg [25], hammering [26], etc). In cyclic tasks, the energy can be stored in the spring during negative work and then released when power generation is required. However, this study mainly focuses on designing and analyzing the EEM system and presenting an adaptive robust controller for controlling the equilibrium position and vibration of the ESEM system. Here, a hybrid scheme combines the fuzzy input shaping (FIS) and the backstepping adaptive enhanced fuzzy sliding mode control (BAEFSMC) is presented. A newly vibration control method based on the concept of [8], the simple and fast response fuzzy input shaping technique is designed for the characteristics of the ESEM system. A fuzzy logic engine is embedded to turn the parameters of the IS according to the stiffness regulation of the VSA system and the cylinder actions to maintain the robustness of the IS in suppressing the residual vibration. To enable the effectiveness of the FIS, the manipulator must track to the shaped position reference. Therefore, the actuator dynamics are considered in control design to analyze the complex high order model of the ESEM system to reduce the influence of the nonlinear characteristics of the hydraulic subsystem as well as the derivative action in the controller. The backstepping technique [27] is used to decompose the plant into two subsystems. The AEFSSMC [28] is embedded for each loop to reduce the system's order and to ensure that the system's state variables, the manipulator position, and the cylinder torque, reach and stay on a sliding surface so that the robustness and the accuracy can be increased. A transition width is applied to the SMC to get rid of the chattering phenomenon in the control signal. An adaptive law is obtained in the sense of

the Lyapunov stability theorem to estimate the optimal value of translation width to confront the system uncertainties online [28].

1.3 Thesis Outline

This thesis begins with a general introduction and literature at chapter 1. In chapter 2, the proposed system hardware is presented. The structure and working principle of the ESEM as well as the VSA are introduced. In addition, the mathematical model of the ESEM is expounded which includes the hydraulic actuator dynamics. The hybrid control system design for position and vibration control is shown in chapter 3. Experimental results for the variation performance of the VSA system and three case studies can be found in chapter 4. Finally, some conclusions and discussions for future works are provided in chapter 5.

**PROPOSED ELECTROHYDRAULIC SERIES ELASTIC MANIPULATOR SYSTEM WITH A
NOVEL VARIABLE STIFFNESS ACTUATOR**

2.1 Background of a hydraulic system

2.1.1 Characteristics of hydraulic systems

Hydraulic systems have many advantages, such as:

- Fast response in acceleration, deceleration and reversal
- High power specific
- Overloading protection
- High efficiency
- Less noise
- Less maintenance requirement
- Both linear and rotary actuators are available

Besides advantages, hydraulic systems have disadvantages as follows:

- High cost of hydraulic components
- Fire and explosion hazards
- Control problem

2.1.2 Applicability of hydraulic systems

Because of the above advantages, hydraulic systems have been widely employed in industrial and mobile applications. The most suitable fields for employing hydraulic systems are shown as following:

- Where relative large torques/forces are required such as industrial press, construction machinery, traction, excavator, wheel loader, *etc*,
- Where fast, stiff response of the resisting load is needed such as machine tool drive, rolling mill, wood processing, *etc*,
- Where accurate control of response is necessary such as control systems in aircraft, industrial robot, *ect*,

- Where manual control with substantial forces/torques are essential such as heavy machine, automotive steering system, *ect*,

Up to now, the use of hydraulic systems in industrial robotic is normally for the rigid manipulators. In the scenarios when robots need to physically interact with environment or people, instability may occur during the interaction if the actuators are too stiff. This would further lead to possible damage of robot or even injuries to staff. While our humans could perform these interactive tasks well, by properly adjusting muscle stiffness of our joints to a level appropriate for the task and the environment. Consider that human-like performance would enable robots to perform better for interactive tasks. Therefore, desired to employ human muscle like variable stiffness actuator (VSA) to concurrently guarantee both safety and performance. It brings in a mechanical compliance that can be adjusted via control action in the joint actuation.

2.2 Electrohydraulic servo system

A concept of electrohydraulic servo system which is utilized as a major power source in the proposed ESEM system is shown in Figure 4. This EHS system consists of a gear pump, an AC motor, a reservoir, a proportional servo valve, and a single hydraulic cylinder. The new generation of proportional servo valve with integrated digital electronics is used in this ESEM system to get rid of some disadvantages of the conventional hydraulic system such as pressure drop through the valve, low bandwidth, low step response time. The AC motor is operated at a constant speed to keep the supply pressure always at the desired working value. The valve spool is controlled to supply pressured oil in both directions to result in the desired force/position at the cylinder.

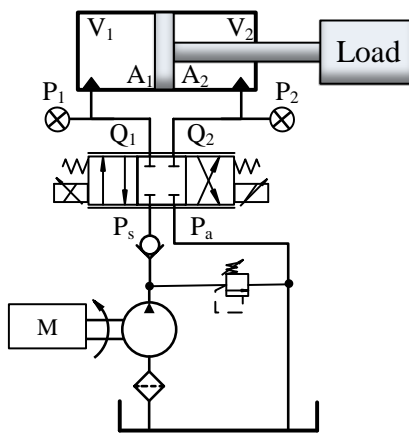


Figure 4 Structure of the electrohydraulic servo system

2.3 Series elastic manipulator with a novel variable stiffness actuator

2.3.1 Background of variable stiffness actuator

This part addresses literature of variable stiffness actuated robots aiming at precise, sensitive, robust, and dynamic interaction with their environment and especially humans. The focus is the adjustment of impedance properties, namely adjusting the robot equilibrium position, the stiffness, and damping. One way of introducing compliance is by using passive elastic elements, like mechanical springs in Figure 5 or pneumatic systems in Figure 6 [29, 30]. It provides a passive elasticity implemented by spring elements at the end effector of a rigid robot. Another way of realizing compliant behavior is by an active compliance. This approach finds application in robots which are equipped with torque sensors in the robot joints shown in Figure 7. Torque sensory information is feedback in a control loop to generate the compliant behavior artificially [31]. Both approaches have considerable advantages. Elastic elements provide mechanical energy storage and thereby enable dynamic behavior and mechanical robustness. Active compliance generated by feedback controllers shows great adaptability regarding stiffness adjustment or choice of task coordinate frame. An approach to integrate the best of both methods is variable stiffness actuation.

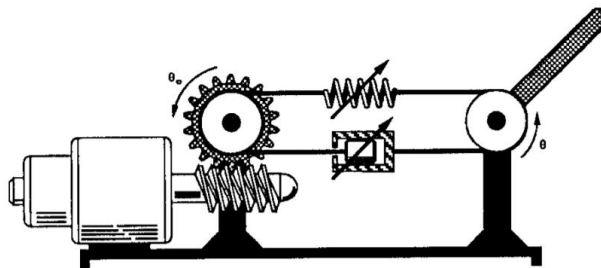


Figure 5 Manipulator with programmable passive impedance

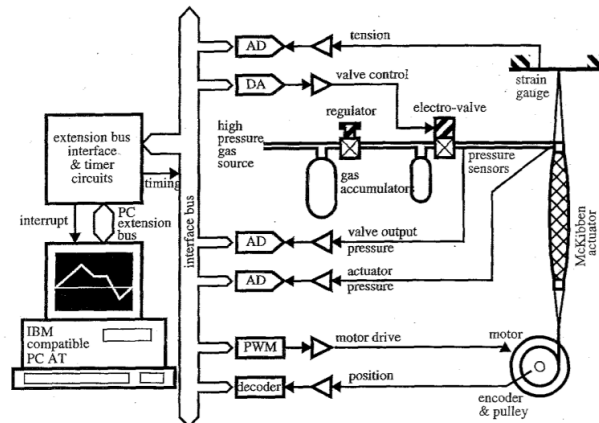


Figure 6 McKibben artificial muscle

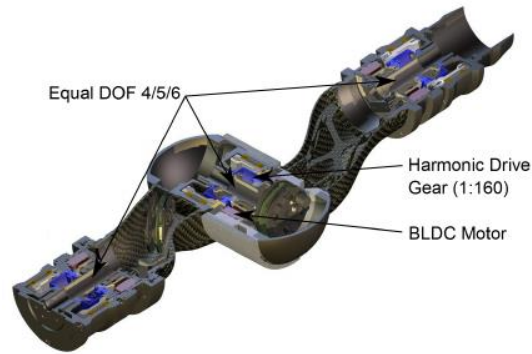


Figure 7 DLR light-weight robot

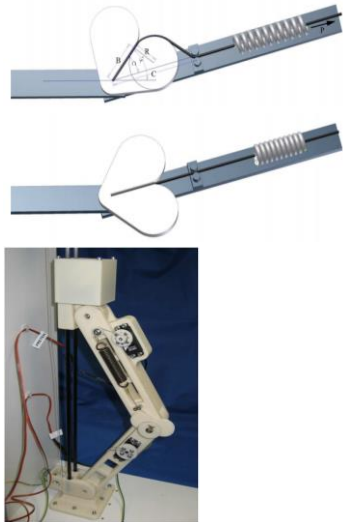
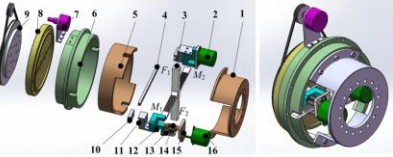
A further advancement of this technology is the recently developed variable stiffness robots. There, the main feature is the deliberate introduction of a mechanically variable, elastic element in the robot joints. A further important property of the elastic elements is its joint torque sensing capability. The variable stiffness actuator (VSA) technology is an advancement of the flexible joint technology of torque controlled lightweight robots (LWRs) [32]. The joints of the LWRs show a mechanical compliance originated mainly by the gearboxes and the torque measurement devices. Furthermore, an additional actuator is introduced as not only the joint position/torque has to be set, but also the joint stiffness itself. A key factor enabling the advantages is the separated structure, where the motor is detached from the link by the elastic element. It provides a certain decoupling whereby the individual properties of the two subsystems can be exploited. The main goals and advantages of the VSA technology are:

- **Mechanism robustness.** The mechanism robustness with respect to external impacts can be increased as the link mass and joint elasticity yield a mechanical low-pass filter. This is especially relevant for fragile mechanisms as fingers of robotic hands, where rigid impacts occur on a regular basis.
- **Increased dynamic performance and energy efficiency.** The ability to store mechanical energy can be exploited to overcome motor velocity limitations. Advanced dynamic capabilities like throwing can be achieved. Some legged robots exploit this fact, too. Additionally, it can be used to increase the energy efficiency during repetitive motion tasks.
- **Task adaptability.** The variability of the stiffness characteristics allows to adapting the system to tasks on a mechanical level. For this so-called task embodiment, the joint stiffness is tuned such that minimal active control influence is necessary to achieve a task.

2.3.2 Proposed variable stiffness actuator for series elastic manipulator

In recent years, many types of research have been conducted to design new VSAs, such as actuators with adjustable stiffness (AwAS) [3], [4], vsaUT-II [5], and vsaMGR [6]. AwAS uses electric motors, springs, and ball screws; VSAUT-II uses electric motors, a spring, and a planetary gear; and vsaMGR combines gear teeth and a flexible beam in a flexible rack. In these VSAs, the equilibrium position is controlled by an electric motor, which guarantees fast performance. But their torque and force depend on the size of the actuator. The advantages and disadvantages comparison of the proposed VSA with the existing prototypes is shown in the table below.

Table 1 Characteristics comparison of VSA systems

Prototype	Schematic	Characteristics	
		Advantages	Disadvantages
The MACCEPA 2.0 [2]		<ul style="list-style-type: none"> - The design is simple with the shape of the profile disk allowing the torque-angle curve can be modified. - The spring is also easy to be replaced for flexible tasks. 	<ul style="list-style-type: none"> - The motors could be a drawback for applications requiring a large torque/force generator. - The complex stiffness controller is needed for disturbance causing by the series connection.
The Modified Gear-rack (MGR) [6]		<ul style="list-style-type: none"> - The structure can provide an accurate regulation against disturbance. - Fast stiffness regulation response. 	<ul style="list-style-type: none"> - The elastic elements are hard to be replaced for different tasks. - The design is a complex mechanism. - Using many actuators and sensors for stiffness regulating. - Requiring a complicated controller for the stiffness control.

<p>The variable stiffness rotational joint [1]</p>		<ul style="list-style-type: none"> - The design is simple providing a wide variety of joint stiffness curves, a high correlation between commanded and measured values. - The springs are easy to be replaced for flexible tasks. 	<ul style="list-style-type: none"> - The motors could be a drawback for applications requiring a large torque/force generator. - The complex stiffness controller is needed for disturbance causing by the series connection.
<p>The AwAS-II [3]</p>		<ul style="list-style-type: none"> - The stiffness changes in a much broader range, fast stiffness regulation response. - The mechanism does not require for a complicated stiffness controller. 	<ul style="list-style-type: none"> - The motors could be a drawback for applications requiring a large torque/force generator. - This design is also complex for springs replacing for flexible tasks.
<p>The 1-DOF variable stiffness actuator [7]</p>		<ul style="list-style-type: none"> - This design is amenable to more compact implementation, - The stiffness can be varied rapidly and continuously during task executions. 	<ul style="list-style-type: none"> - Requiring a complicated controller for the stiffness control. - The motors and a timing transmission belt could be a drawback for applications requiring a large torque/force generator.
<p>The proposed VSA system</p>		<ul style="list-style-type: none"> - The major torque generator of the manipulator is hydraulic cylinder which has high power density and high energy efficiency. - The VSA mechanism does not require for a complicated stiffness controller. - The stiffness adjusts in much broader range, high dynamic. - The springs can be easy replaced for different research objectives. 	

Based on the analysis, the proposed VSA system was designed as a combination of the flexible joint and an adjustable spring base mechanism (ASBM) as shown in Figure 8. The ASBM uses a ball screws as a linear motion actuator which has capable of handling large loads, highly precise positioning. The coupling torque acting on the second link has different values for every position of the nut. Not only the moment arms but also the tension of the springs will be adjusted by the nut position. Due to the requirement of working condition, the DC motor drives the ball screws to provide the desired stiffness. As a result, the VSA has an ability to change the stiffness in much broader range, high dynamic because the primary torque generator and the VSA are two separate units, they do not affect each

other while operating. In addition, the disturbance torque acting on the DC motor which causes by these two springs is not significant due to the high transmission ratio. Thus, the VSA system is not required for a complicated controller. The springs in this design are also easy to be replaced for different research objectives.

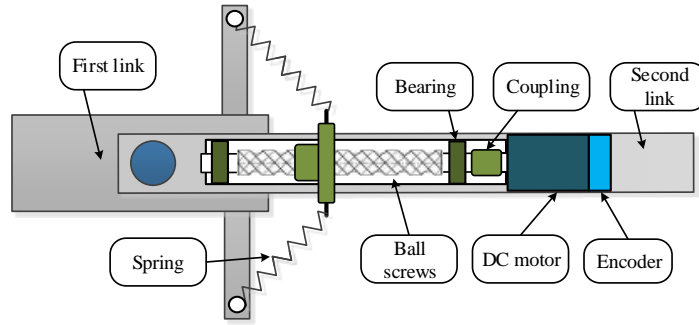


Figure 8 Proposed variable stiffness actuator

2.4 System mathematical modeling

2.4.1 Model of electrohydraulic servo valve system

Using the principles of hydraulic system, the governing nonlinear equations describing the fluid flow distribution in the valve are written as [33]

$$Q_1 = \begin{cases} C_d w x_s \sqrt{\frac{2}{\rho} (p_s - p_1)}, & x_s \geq 0 \\ C_d w x_s \sqrt{\frac{2}{\rho} (p_1 - p_a)}, & x_s \leq 0 \end{cases} \quad (1)$$

$$Q_2 = \begin{cases} C_d w x_s \sqrt{\frac{2}{\rho} (p_2 - p_a)}, & x_s \geq 0 \\ C_d w x_s \sqrt{\frac{2}{\rho} (p_s - p_2)}, & x_s \leq 0 \end{cases} \quad (2)$$

where Q_1 and Q_2 represent fluid flows into and out of the valve, respectively. C_d is the orifice coefficient of discharge, ρ is the mass density of the fluid, p_s is the pump pressure, and p_a is the return pressure. w is the area gradient that relates the spool displacement (x_s) to the orifice area. The continuity equations for oil flow through the cylinder, are

$$\dot{p}_1 = \frac{\beta}{V_{o1} + A_1 x_p} (Q_1 - A_1 \dot{x}_p - Q_L) \quad (3)$$

$$\dot{p}_2 = \frac{\beta}{V_{02} - A_2 x_p} (-Q_2 + A_2 \dot{x}_p + Q_L) \quad (4)$$

here β is the effective bulk modulus of the hydraulic fluid, and V_{01} and V_{02} are the initial volumes of fluid trapped at the sides of the actuator. The spool displacement, x_s , is considered to be proportional to the input voltage, u .

$$x_s = k_{sp} u \quad (5)$$

2.4.2 Model of variable stiffness actuator

Based on the forces analysis in Figure 9, the spring forces acting on the ball screws nut can be obtained as

$$F_n = F_{s1x} + F_{s2x} = F_{s1} \cos \beta_1 + F_{s2} \cos \beta_2 \quad (6)$$

with β_1 and β_2 are defined in (26)

The proposed design uses ball screws with length $L = 50$ mm, ball screw lead $s = 2$ mm. The load torque required for the actuator is

$$T_L = \frac{F_n s}{2\pi\eta} = \frac{0.002 F_n}{2\pi 0.9} \quad (7)$$

The power supplier chosen for the proposed VSA system is a DC motor IG-36PGM 06TYPE with reduction ratio

$$n = 5:1$$

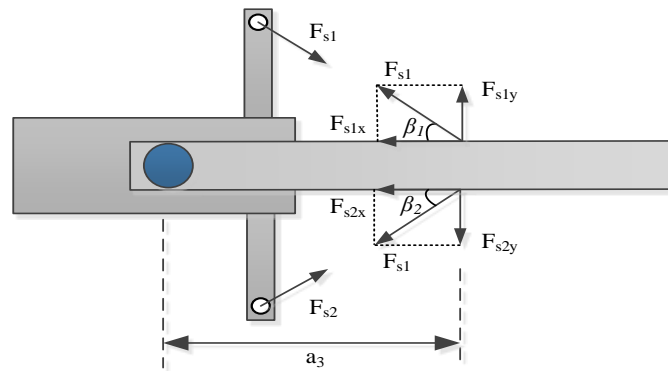


Figure 9 VSA forces analysis

2.4.3 Model of series elastic manipulator

A manipulator is a mechanical device which can operate remote objects or material even in the absence of any worker. Links and joints make a long chain in a manipulator, which can manipulate in its workspace. The total number of joints gives the degrees-of-freedom (DOF). Manipulators are classified into two types namely:

- Parallel manipulator
- Serial manipulator

Most industrial robots are the serial manipulators which are designed as a series of links connected by motor actuated joints from base part to end effector part. These types of manipulators have an anthropomorphic arm structure with a shoulder, an elbow, and a wrist. The main application for these serial type manipulators in present industry is picking and placing assembly robot.

The simple form of the ESEM system is shown in Figure 10 with link-frame and parameters assignment for each link. In order to compute the position and orientation of the manipulator's end effector relative to the base of the manipulator as a function of the joint variables, the link's parameters are assumed as

- a_i is the distance from Z_i to Z_{i+1} measured along X_i
- α_i is the angle from Z_i to Z_{i+1} measured along X_i
- d_i is the distance from X_{i-1} to X_i measured along Z_i
- θ_i is the angle from X_{i-1} to X_i measured along Z_i

The corresponding link's parameters are shown in Table 2. Substituting these parameters into the general form of transformation operator [34] presented in (8).

$${}^{i-1}T_i = \begin{bmatrix} \cos \theta_i & -\sin \theta_i & 0 & a_{i-1} \\ \sin \theta_i \cos \alpha_{i-1} & \cos \theta_i \cos \alpha_{i-1} & -\sin \alpha_{i-1} & -\sin \alpha_{i-1} d_i \\ \sin \theta_i \sin \alpha_{i-1} & \cos \theta_i \sin \alpha_{i-1} & \cos \alpha_{i-1} & \cos \alpha_{i-1} d_i \\ 0 & 0 & 0 & 1 \end{bmatrix} \quad (8)$$

$${}^0T_1 = \begin{bmatrix} \cos \theta_1 & -\sin \theta_1 & 0 & 0 \\ 0 & 0 & -1 & 0 \\ \sin \theta_1 & \cos \theta_1 & 0 & 0 \\ 0 & 0 & 0 & 1 \end{bmatrix} \quad (9)$$

$${}^1_2T = \begin{bmatrix} \cos \theta_2 & -\sin \theta_2 & 0 & l_1 \\ \sin \theta_2 & \cos \theta_2 & 0 & 0 \\ 0 & 0 & 1 & 0 \\ 0 & 0 & 0 & 1 \end{bmatrix} \quad (10)$$

$${}^2_3T = \begin{bmatrix} 1 & 0 & 0 & l_2 \\ 0 & 1 & 0 & 0 \\ 0 & 0 & 1 & 0 \\ 0 & 0 & 0 & 1 \end{bmatrix} \quad (11)$$

Table 2 Link parameters of the two-link planar manipulator

i	α_{i-1}	a_{i-1}	d_i	θ_i
1	90	0	0	θ_1
2	0	l_1	0	θ_2
3	0	l_2	0	0

The transformation, 0_3T , will be a function of all 2 joint variables.

$${}^0_3T = {}^0_1T {}^1_2T {}^2_3T \quad (12)$$

$${}^0_3T = \begin{bmatrix} \cos \theta_1 \cos \theta_2 - \sin \theta_1 \sin \theta_2 & -\cos \theta_1 \sin \theta_2 - \sin \theta_1 \cos \theta_2 & 0 & l_2 (\cos \theta_1 \cos \theta_2 - \sin \theta_1 \sin \theta_2) + l_1 \cos \theta_1 \\ 0 & 0 & -1 & 0 \\ \cos \theta_1 \sin \theta_2 + \sin \theta_1 \cos \theta_2 & \cos \theta_1 \cos \theta_2 - \sin \theta_1 \sin \theta_2 & 0 & l_0 + l_2 (\cos \theta_1 \sin \theta_2 + \sin \theta_1 \cos \theta_2) + l_1 \sin \theta_1 \\ 0 & 0 & 0 & 1 \end{bmatrix}$$

$$= \begin{bmatrix} \cos(\theta_1 + \theta_2) & -\sin(\theta_1 + \theta_2) & 0 & l_2 (\cos(\theta_1 + \theta_2)) + l_1 \cos \theta_1 \\ 0 & 0 & -1 & 0 \\ \sin(\theta_1 + \theta_2) & \cos(\theta_1 + \theta_2) & 0 & l_0 + l_2 (\sin(\theta_1 + \theta_2)) + l_1 \sin \theta_1 \\ 0 & 0 & 0 & 1 \end{bmatrix} \quad (13)$$

The coordination of the end effector is obtained as

$$X = \begin{bmatrix} l_2 (\cos(\theta_1 + \theta_2)) + l_1 \cos \theta_1 \\ 0 \\ l_0 + l_2 (\sin(\theta_1 + \theta_2)) + l_1 \sin \theta_1 \end{bmatrix} \quad (14)$$

Jacobian matrices are widely used to describe the kinematics and inverse kinematics of the end-effector motion in the conventional Cartesian coordinate system, and the Jacobian matrix for the manipulator is given as follows:

$$\begin{aligned} \dot{X} &= J\dot{\theta} \\ \ddot{X} &= J(\theta)\ddot{\theta} + \dot{J}(\theta)\dot{\theta} \end{aligned} \quad (15)$$

$$J = \begin{bmatrix} \frac{\partial X_x}{\partial \theta_1} & \frac{\partial X_x}{\partial \theta_2} \\ \frac{\partial X_y}{\partial \theta_1} & \frac{\partial X_y}{\partial \theta_2} \end{bmatrix} = \begin{bmatrix} -l_1 \sin \theta_1 - l_2 \sin(\theta_1 + \theta_2) & -l_2 \sin(\theta_1 + \theta_2) \\ l_1 \cos \theta_1 + l_2 \cos(\theta_1 + \theta_2) & l_2 \cos(\theta_1 + \theta_2) \end{bmatrix}$$

The closed-form dynamic equations for the two-link planar manipulator shown in Figure 10 is computed based on [34]. For simplicity, the mass distribution is assumed extremely simple, all mass exists as a point mass at the distal end of each link, m_1 and m_2 are the mass of first link and second link, respectively. The torque at the actuators which is a function of joint position, velocity and acceleration are expressed as (16)

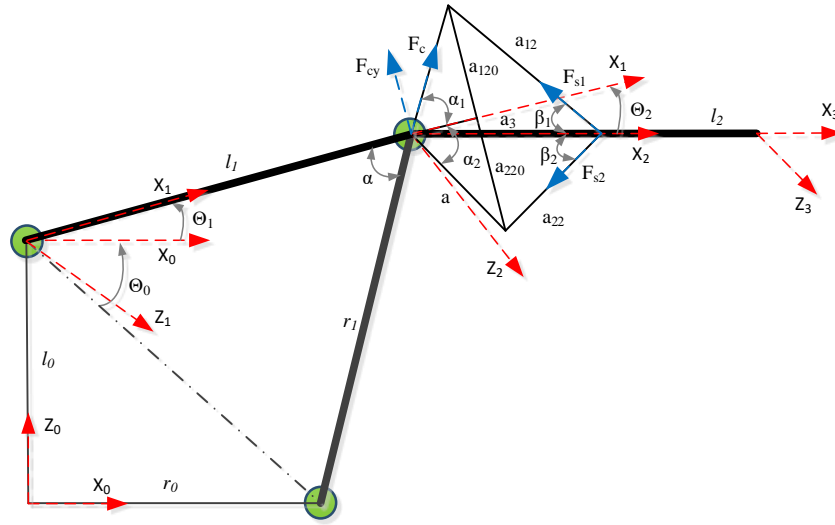


Figure 10 System parameters assignment

$$M(\theta)\ddot{\theta} + R(\theta, \dot{\theta}) + I(\theta) = T \quad (16)$$

with

$$M(\theta) = \begin{bmatrix} J_1 + J_2 + m_2 l_1^2 + 2m_2 l_1 d_2 \cos \theta_2 & J_2 + m_2 l_1 d_2 \cos \theta_2 \\ J_2 + m_2 l_1 d_2 \cos \theta_2 & J_2 \end{bmatrix},$$

$$R(\theta, \dot{\theta}) = \begin{bmatrix} -m_2 l_1 d_2 \sin \theta_2 (\dot{\theta}_2^2 + 2\dot{\theta}_1 \dot{\theta}_2) \\ m_2 l_1 d_2 \sin \theta_2 \dot{\theta}_1^2 \end{bmatrix},$$

$$I(\theta) = \begin{bmatrix} g(m_1 d_1 + m_2 l_1) \cos \theta_1 + g m_2 d_2 \cos(\theta_1 + \theta_2) \\ g m_2 d_2 \cos(\theta_1 + \theta_2) \end{bmatrix},$$

$$\theta = [\theta_1 \quad \theta_2]^T, \quad \dot{\theta} = [\dot{\theta}_1 \quad \dot{\theta}_2]^T, \quad \ddot{\theta} = [\ddot{\theta}_1 \quad \ddot{\theta}_2]^T, \quad T = [T_1 \quad T_2]^T.$$

where T_1 and T_2 are the two torque inputs, and $\ddot{\theta}_1$ and $\ddot{\theta}_2$ are the acceleration outputs. g is the acceleration of gravity, m_i is the weight of the link i , and J_i is the moment of inertia about an axis through the center of mass of link i .

From Figure 10, the relationship between first link angle, θ_1 , and cylinder displacement, x_p , can be expressed as

$$\cos(\theta_0 + \theta_1) = \frac{l_1^2 + l_0^2 + r_0^2 - (l_{cyl} + x_p)^2}{2l_1 \sqrt{(l_0^2 + r_0^2)}} \quad (17)$$

The first excited torque, τ_1 , which is generated by the cylinder can be calculated by

$$\tau_1 = l_1 F_{cy} = l_1 F_c \sin \alpha \quad (18)$$

where

$$F_c = A_1 p_1 - A_2 p_2 \quad (19)$$

$$\cos \alpha = \frac{l_1^2 + r_1^2 - l_0^2 - r_0^2}{2l_1 r_1} \quad (20)$$

From the flexible joint design, the two springs k_1 and k_2 connect the first link and the second link through a nut of a ball screws. The DC motor drives the screws to change a_3 to provide a suitable stiffness for the system. The forces are generated by these two springs are:

$$F_{s,i} = \Delta x_i k_i \quad (21)$$

$$F_{s2} = \Delta x_2 k_2 \quad (22)$$

where

$$\begin{cases} \Delta x_1 = \sqrt{a^2 + a_3^2 - 2aa_3 \cos(\alpha_1 + \theta_2)} - a_{120} \\ \Delta x_2 = \sqrt{a^2 + a_3^2 - 2aa_3 \cos(\alpha_2 - \theta_2)} - a_{220} \end{cases} \quad (23)$$

The second torque τ_2 and the coupling torque τ_{12} can be calculated as

$$\tau_2 = (F_{s1} \sin \beta_1 - F_{s2} \sin \beta_2) a_3 \quad (24)$$

$$\tau_{12} = (F_{s1} \sin \beta_1 - F_{s2} \sin \beta_2) (l_1 + a_3) \quad (25)$$

where

$$\begin{cases} \beta_1 = \cos^{-1} \left(\frac{a_3^2 + a_{12}^2 - a^2}{2a_3 a_{12}} \right) \\ \beta_2 = \cos^{-1} \left(\frac{a_3^2 + a_{22}^2 - a^2}{2a_3 a_{22}} \right) \end{cases} \quad (26)$$

From (18), (24) and (25) the torque input vector is achieved by:

$$\begin{bmatrix} T_1 \\ T_2 \end{bmatrix} = \begin{bmatrix} \tau_1 - \tau_{12} \\ \tau_2 \end{bmatrix} \quad (27)$$

The angular acceleration $\ddot{\theta}_1$ can be obtained from (16) as

$$\ddot{\theta}_1 = \bar{B}(\theta_2) T_1 + \bar{F}(\theta_1, \dot{\theta}_1, \theta_2, \dot{\theta}_2) + d_1(t) \quad (28)$$

with

$$\bar{B} = \frac{J_2}{J_1 J_2 + J_2 l_1^2 m_2 - (d_2 l_1 m_2 c \theta_2)^2},$$

$$\bar{F} = \frac{J_2(d_2\dot{\theta}_2 l_1 m_2 s\theta_2(\dot{\theta}_2 + 2\dot{\theta}_1) - gc\theta_2(d_1 m_1 + l_1 m_2) - d_2 g m_2 c(\theta_1 + \theta_2))}{J_1 J_2 + J_2 l_1^2 m_2 - (d_2 l_1 m_2 c\theta_2)^2} + \frac{(J_2 + d_2 l_1 m_2 c\theta_2)(d_2 l_1 m_2 s\theta_2 \dot{\theta}_1^2 + d_2 g m_2 c(\theta_1 + \theta_2))}{J_1 J_2 + J_2 l_1^2 m_2 - (d_2 l_1 m_2 c\theta_2)^2}$$

$d_1(t)$ is the uncertainties in the mechanical subsystem of the ESEM system. The uncertainties consist of the coupling torques, frictions, and parametric uncertainties.

The time derivative of T_l is calculated as

$$\begin{aligned} \dot{T}_l &= l_1 \sin(\alpha)(A_1 \dot{p}_1 - A_2 \dot{p}_2) + l_1 F_c \cos(\alpha) - \Delta \dot{F}(l_1 + a_3) \\ &= \bar{K}(x_p, \dot{x}_p, \theta_2) + u \bar{H}(x_p, p_1, p_2, \theta_2) + d_2(t) \end{aligned} \quad (29)$$

where

$$\bar{K} = -\beta l_1 \sin(\alpha) \dot{x}_p \left(\frac{A_1^2}{V_{01} + A_1 x_p} + \frac{A_2^2}{V_{02} - A_2 x_p} \right),$$

$$\bar{H} = \beta C_d w l_1 k_{sp} \sin(\alpha) \sqrt{\frac{2}{\rho}} \left(\frac{A_1 \sqrt{\Delta P_p}}{V_{01} + A_1 x_p} + \frac{A_2 \sqrt{\Delta P_r}}{V_{02} - A_2 x_p} \right),$$

$$\Delta P_p = \begin{cases} (p_s - p_1) & \text{if } u \geq 0 \\ (p_1 - p_a) & \text{if } u < 0 \end{cases}, \quad \Delta P_r = \begin{cases} (p_2 - p_a) & \text{if } u \geq 0 \\ (p_s - p_2) & \text{if } u < 0 \end{cases}.$$

and $d_2(t)$ is the uncertainties in the hydraulic subsystem that are the leakages, cylinder friction, parametric uncertainties, and the modeling error.

The state variables of the system are defined as $x = [x_1 \ x_2 \ x_3]^T = [\theta_l \ \dot{\theta}_l \ T_l]^T$. Then, the plant can be described by

the following state spaces.

$$\begin{cases} \dot{x}_1 = x_2 \\ \dot{x}_2 = \bar{B}x_3 + \bar{F} + d_1(t) \\ \dot{x}_3 = u \bar{H} + \bar{K} + d_2(t) \end{cases} \quad (30)$$

3.1 Overview of the hybrid controller

For the vibration and position control purpose, the main objective of the proposed controller is to generate the electric signal to the servo valve, u , to achieve the desired output which are the position of the manipulator, θ_1 , and the residual vibration of the end effector, θ_2 . The overall scheme of the proposed controller is presented in Figure 11. The hybrid controller contains two parts, the first part using a newly vibration control algorithm to shape the reference signal which results in vibration suppression for the end effector. Meanwhile, the second part utilizing backstepping technique [27] for the defined state spaces (30) is decomposed into two loops. The outer loop controls trajectory of the manipulator with the output is the virtual torque. The inner loop guarantees the torque stability of the hydraulic subsystem. In each loop, an EFSMC system, in which a translation width idea is embedded into the FSMC is applied. Moreover, to confront the uncertainties existed in practical applications, an adaptive tuner, which is derived in the sense of the Lyapunov stability theorem, is utilized to adjust the EFSMC parameter for further assuring robust and optimal control performance.

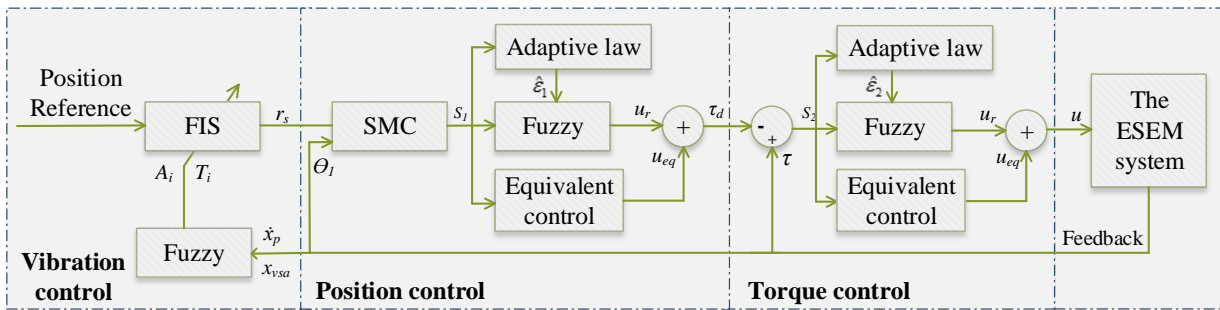


Figure 11 Structure of the hybrid controller

3.2 Design of Adaptive Input Shaping

3.2.1 Conventional Input Shaper - ZV and ZVD

Between the late 50's and the publication of the input shaping technique (IST) paper by Singer and Seering [8], there was some work on the shaping of input profiles for control of residual vibration [35], [36]. Swigert [36] proposed techniques for the determination of torque profiles which considered the sensitivity of the terminal states to variations

in the model parameters. Publication of the IST paper renewed interest in profiteering reference inputs for robust vibration control, which has resulted in dozens of papers with application to spacecraft, robots, cranes, chemical processes, *etc.*

As a first step to understanding how to generate commands that move systems without vibration, it is helpful to start with the simplest such command. By giving a system an impulse will cause it to vibrate; however, if we apply the second impulse to the system at the right time, we can cancel the vibration induced by the first impulse. This concept is shown in Figure 12.

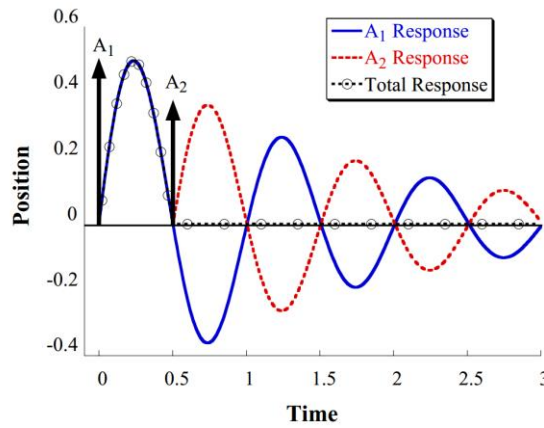


Figure 12 Two impulse response

As shown in Figure 12, it is important to derive the amplitudes of the impulse, A_1 and A_2 , and its time location T_1 and T_2 . If we have properly value of the system's natural frequency, ω_n , and damping ratio, ζ , then the residual vibration that results from a sequence of impulses can be described by [37]:

$$V(\omega, \zeta) = e^{-\zeta\omega T_n} \sqrt{C(\omega, \zeta)^2 + S(\omega, \zeta)^2} \quad (31)$$

where

$$C(\omega, \zeta) = \sum_{i=1}^n A_i e^{\zeta\omega T_i} \cos(\omega_d T_i), \quad (32)$$

$$S(\omega, \zeta) = \sum_{i=1}^n A_i e^{\zeta\omega T_i} \sin(\omega_d T_i)$$

A_i and t_i are the amplitudes and time locations of the impulses, n is the number of impulses in the impulse sequence, and $\omega_d = \omega_n \sqrt{1 - \zeta^2}$. (31) is actually the percentage residual vibration. It presents how much vibration a sequence of impulses will cause. By setting (31) equal to zero, we can solve for the impulse amplitudes and time locations that would lead to zero residual vibration. However, we must place a few more restrictions on the impulses, or the solution will converge to zero-valued or infinitely valued impulses. To avoid the trivial solution of all zero-valued impulses and to obtain a normalized result, we require the impulses to sum to one:

$$\sum A_i = 1 \quad (33)$$

For a two-impulse sequence, the problem has four unknowns, the two impulse amplitudes (A_1, A_2) and the two impulse time locations (T_1, T_2). Without loss of generality, we can set the time location of the first impulse equal to zero, $T_1 = 0$. The problem is now reduced to finding three unknowns (A_1, A_2, T_2). In order for (31) to equal zero, the expressions in (32) must both equal zero independently

$$0 = A_1 + A_2 e^{\zeta \omega_d T_2} \cos(\omega_d T_2) \quad (34)$$

$$0 = A_2 e^{\zeta \omega_d T_2} \sin(\omega_d T_2) \quad (35)$$

By solving these above constraints, the sequence of two impulses which refers as zero-vibration (ZV) shaper that leads to zero residual vibration can now be summarized as [8]:

$$\begin{aligned} T_1 &= 0, & T_2 &= \frac{\pi}{\omega_d}, \\ A_1 &= \frac{1}{1 + e^{\frac{-\zeta \pi}{\sqrt{1 - \zeta^2}}}}, & A_2 &= \frac{e^{\frac{-\zeta \pi}{\sqrt{1 - \zeta^2}}}}{1 + e^{\frac{-\zeta \pi}{\sqrt{1 - \zeta^2}}}} \end{aligned} \quad (36)$$

As presented in (36), these parameters of ZV shaper depend on the system's natural frequency, ω_n , and damping ratio, ζ , which are hard to obtain exactly in a practical system. This may lead to the residual vibration will not result in zero. In order to increase the robustness of input shaping, the shaper must satisfy an additional constraint. One such constraint sets the derivative of (31), with respect to frequency, equal to zero

$$0 = \frac{d}{d\omega} V(\omega, \zeta) \quad (37)$$

Another IST called a zero vibration and derivative (ZVD) shaper is presented as follows

$$\begin{aligned}
 T_1 &= 0, & T_2 &= \frac{\pi}{\omega_d}, & T_3 &= \frac{2\pi}{\omega_d} \\
 A_1 &= \frac{1}{1 + 2e^{\frac{-\zeta\pi}{\sqrt{1-\zeta^2}}} + e^{\frac{-2\zeta\pi}{\sqrt{1-\zeta^2}}}}, & A_2 &= \frac{2e^{\frac{-\zeta\pi}{\sqrt{1-\zeta^2}}}}{1 + 2e^{\frac{-\zeta\pi}{\sqrt{1-\zeta^2}}} + e^{\frac{-2\zeta\pi}{\sqrt{1-\zeta^2}}}}, & A_3 &= \frac{e^{\frac{-2\zeta\pi}{\sqrt{1-\zeta^2}}}}{1 + 2e^{\frac{-\zeta\pi}{\sqrt{1-\zeta^2}}} + e^{\frac{-2\zeta\pi}{\sqrt{1-\zeta^2}}}}
 \end{aligned} \quad (38)$$

The examples of impulse sequence convolved with a pulse signal are shown in Figure 13. In practical application, there always exist errors in system's parameters identification, and the ZV shaper is very sensitive to modeling errors since small deviations from the modeling frequency can lead to large amounts of residual vibration. Figure 14 presents the robustness comparison of some shapers called sensitivity curves [8].

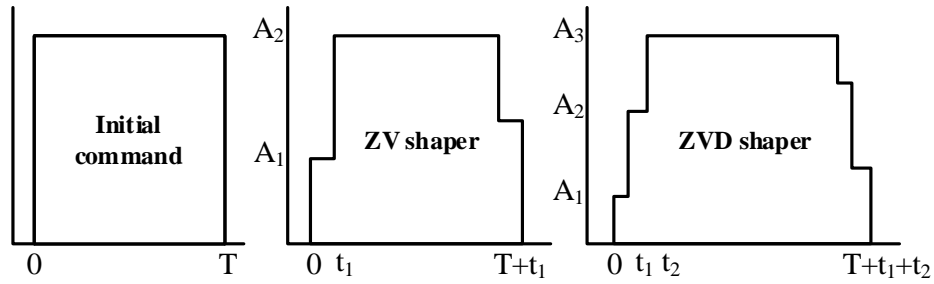


Figure 13 Continuous shaper input

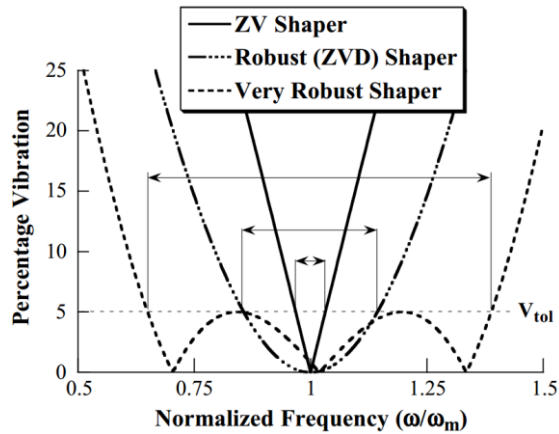


Figure 14 Sensitivity curves

3.2.2 Proposed Adaptive Input Shaping

If the estimated values are close to the actual values, the ZV shaper results in an excellent vibration suppression. However, as can be seen in Figure 14, the percentage of vibration is increased rapidly if the system's parameters are out of acceptable range of 5% insensitivity. Due to the working condition, the VSA adjusts the stiffness along with system parameters (ω and ζ) in a wide range. Even with the (ZVD) shaper which is more robust to the modeling errors than ZV, cannot perform well in such a large deviation of actual frequency and modeling frequency. The FIS is designed in this section that is able to update the IS parameters during the stiffness varying of the manipulator to keep the estimated values as close to the actual values. As a result, The ZV remains the percentage vibration under the desired value.

First, the ESEM was executed without IS at some positions of the VSA system to collect the oscillation response of the end effector. The signal was analyzed by the spectral estimation toolbox of MATLAB and [37] to obtain the ZV parameters. Based on the analysis, the designed parameters of the model and the behavior of the ESEM system, the fuzzy input/output MFs were chosen as Figure 15. Let the position of the ball screws nut, x_{vsa} , and cylinder velocity, \dot{x}_p , be the input linguistic variable of the fuzzy logic, the ZV parameters, A_i and T_i be the output. Triangular type input membership functions (MFs) with fuzzy sets P0, P1, P2, P3, P4, P5 and output MFs with fuzzy sets T0E, T0R, T1E, T1R, T2E, T2R, T3E, T3R, T4E, T4R, T5E, T5R, A1E, A2E, A1R, A2R are shown in Figure 15 for the proposed FIS. The rule table is finally designed and shown in Table 3.

Table 3 Rule table of the fuzzy inference

FIS Rule	Input 1 - x_{vsa}					
	P0	P1	P2	P3	P4	P5
Input 2 - \dot{x}_p						
Extend	A1E	A1E	A1E	A1E	A1E	A1E
	A2E	A2E	A2E	A2E	A2E	A2E
	T0E	T1E	T2E	T3E	T4E	T5E
Retract	A1R	A1R	A1R	A1R	A1R	A1R
	A2R	A2R	A2R	A2R	A2R	A2R
	T0R	T1R	T2R	T3R	T4R	T5R

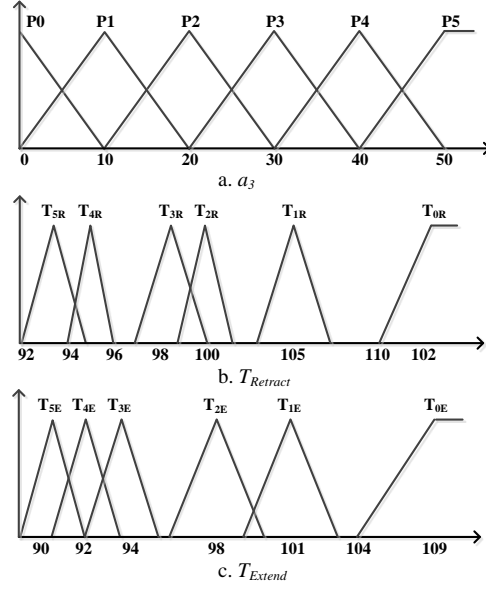


Figure 15 MFs for input/output of the proposed FIS

3.3 Design of Backstepping Adaptive Enhanced Fuzzy Sliding Mode controller

The proposed BAEFSMC system for the ESEM is discussed into two parts. Based on the chosen states of the system, the first part is designed for the outer loop, position control, the second part is utilized for torque control to find the control law for the servo valve so that the manipulator angle can track the desired commands.

Step 1: Design the SMC to guarantee the tracking position error as small as possible. This step will generate the virtual torque control x_{3d} . Choosing the sliding surface as [38]

$$s_1 = c_1 e_1 + e_2 \quad (39)$$

where c_1 is non-zero positive constant, tracking error of first and second state variable: $e_1 = x_1 - x_{1d}$; $e_2 = x_2 - x_{2d}$.

Differentiating (39) with respect to time yields

$$\begin{aligned} \dot{s}_1 &= c_1 \dot{e}_1 + \dot{e}_2 \\ &= c_1 \dot{e}_1 + \bar{B}x_3 + \bar{F} + d_1(t) - \dot{x}_{2d} \end{aligned} \quad (40)$$

Define the torque tracking error as

$$s_2 = x_3 - x_{3d} \quad (41)$$

Using backstepping technique, the equivalent control effort can be derived as the solution of $\dot{s}_l(t)=0$ without considering the uncertainty $d_l(t)$

$$x_{3eq} = \bar{B}^{-1} (\dot{x}_{2d} - c_1 \dot{e}_1 - \Pi_1 s_1 - \bar{F}) \quad (42)$$

where Π_1 is a positive constant.

In order to remedy the chattering phenomenon in the conventional SMC, a fuzzy logic inference mechanism is used to add a translation width, ε_1^* , into the virtual torque control, referred as EFSMC [28]. The design principle is that, when the error states are near the sliding surface, the hitting control effort will vanish to avoid imperfection of actual switching device. On the contrary, while the error states take away from the sliding surface, the translation-width term will be embedded to pull the error states back to the sliding surface rapidly. Let the sliding surface s_l be the input linguistic variable of the fuzzy logic, and let the virtual torque x_{3d} be the output linguistic variable. The fuzzy linguistic rule base can be summarized as follows

Rule 1, If s_l is Positive, then x_{3d} is $x_{3eq} - \varepsilon_1^*$

Rule 2, If s_l is Zero, then x_{3d} is x_{3eq}

Rule 3, If s_l is Negative, then x_{3d} is $x_{3eq} + \varepsilon_1^*$

The triangular membership functions and center average defuzzification method are also adopted in the EFSMC system, and the membership function of x_{3d} is depicted in Figure 16

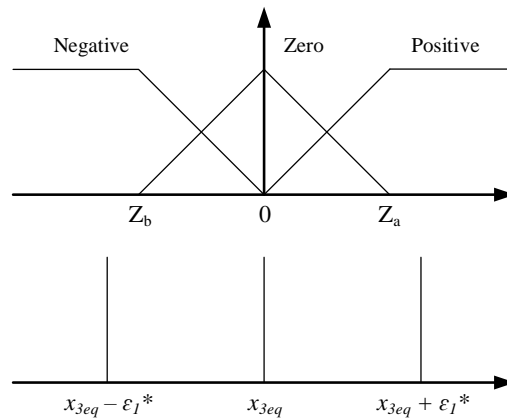


Figure 16 Membership functions of fuzzy sets for EFSMC of outer loop

Then, the control output of the outer loop can be expressed as

$$x_{3d} = w_{11}(x_{3eq} - \mathcal{E}_1^*) + w_{12}x_{3eq} + w_{13}(x_{3eq} + \mathcal{E}_1^*) \quad (43)$$

where $0 \leq w_{11} \leq 1$, $0 \leq w_{12} \leq 1$, $0 \leq w_{13} \leq 1$, are the firing strengths of rules 1)–3), respectively; the relation $w_{11} + w_{12} + w_{13} = 1$ is valid according to the special case of triangular membership functions; (43) can be rewritten as

$$x_{3d} = x_{3eq} - \mathcal{E}_1^*(w_{11} - w_{13}) \quad (44)$$

The virtual torque in (44) can be further analyzed as the following four conditions [39], and only one of four conditions will occur for any value of s_I

- Condition 1: If $s_I > Z_a$ then $w_{11} = 1$; $w_{12} = w_{13} = 0$.

$$x_{3d} = x_{3eq} - \mathcal{E}_1^* \quad (45)$$

- Condition 2: If $0 < s_I \leq Z_a$ then $0 < w_{11}, w_{12} \leq 1$; $w_{13} = 0$.

$$x_{3d} = x_{3eq} - w_{11}\mathcal{E}_1^* \quad (46)$$

- Condition 3: If $Z_b < s_I \leq 0$ then $w_{11} = 0$; $0 < w_{12}, w_{13} \leq 1$.

$$x_{3d} = x_{3eq} + w_{13}\mathcal{E}_1^* \quad (47)$$

- Condition 4: If $s_I \leq Z_b$ then $w_{11} = w_{12} = 0$; $w_{13} = 1$.

$$x_{3d} = x_{3eq} + \mathcal{E}_1^* \quad (48)$$

There exists an optimal translation width, \mathcal{E}_1^* , which can be obtained as (49) to achieve minimum control efforts and match the sliding condition [28]. However, the stability of the control system cannot be guaranteed during the whole control process, and the magnitude of the control effort is deeply affected by the translation width. At the same time, the translation width is related to the magnitude of uncertainties to pull the error states back to the sliding surface. If the translation width is too small, then the tracking-error dynamic trajectory may be away from the sliding surface. Therefore, a conservative control law with a large width is usually selected. Although using a conservative value for

the translation width results in hitting the sliding surface rapidly, it will yield large control efforts such that it is difficult to implement in practical applications.

$$\varepsilon_l^* = \frac{|d_l|}{|w_{11} - w_{13}|} + \gamma_l \quad (49)$$

where γ_l is a small positive constant. In practice, the unknown lumped uncertainties vary flexibly, the optimal translation width, ε_l^* , is impossible to obtain exactly. Thus, an adaptive algorithm is used in this loop to estimate the value of the translation width, and its estimated error is defined as

$$\tilde{\varepsilon}_l(t) = \hat{\varepsilon}_l(t) - \varepsilon_l^* \quad (50)$$

The virtual torque can be represented as

$$\hat{x}_{3d} = x_{3eq} - \hat{\varepsilon}_l(w_{11} - w_{13}) \quad (51)$$

Choose the first Lyapunov candidate as

$$V_l = \frac{s_l^2(t) + \alpha_l \tilde{\varepsilon}_l^2(t)}{2} \quad (52)$$

where α_l is a positive constant. Differentiating V_l with respect to time, then substituting (40)-(42), (49) into it yields

$$\begin{aligned} \dot{V}_l &= s_l(t)\dot{s}_l(t) + \alpha_l \tilde{\varepsilon}_l(t)\dot{\tilde{\varepsilon}}_l(t) \\ &= s_l(t) \left[\bar{B}s_2 - \Pi_l s_l - \hat{\varepsilon}_l(t)(w_{11} - w_{13}) + d_l(t) \right] + \alpha_l \tilde{\varepsilon}_l(t)\dot{\tilde{\varepsilon}}_l(t) \\ &= \bar{B}s_l s_2 - \Pi_l s_l^2 + \alpha_l \tilde{\varepsilon}_l(t)\dot{\tilde{\varepsilon}}_l(t) - s_l(t) \left[\varepsilon_l^*(w_{11} - w_{13}) - d_l(t) + \hat{\varepsilon}_l(t)(w_{11} - w_{13}) - \varepsilon_l^*(w_{11} - w_{13}) \right] \\ &= \bar{B}s_l s_2 - \Pi_l s_l^2 - s_l(t)(w_{11} - w_{13}) \left[\frac{|d_l(t)|}{|w_{11} - w_{13}|} + \gamma_l - \frac{d_l(t)}{(w_{11} - w_{13})} \right] - s_l(t)(w_{11} - w_{13})\tilde{\varepsilon}_l(t) + \alpha_l \tilde{\varepsilon}_l(t)\dot{\tilde{\varepsilon}}_l(t) \\ &\leq \bar{B}s_l s_2 - \Pi_l s_l^2 - s_l(t)\gamma_l(w_{11} - w_{13}) + s_l(t)\tilde{\varepsilon}_l(t)\alpha_l \left[\frac{\dot{\tilde{\varepsilon}}_l(t)}{s_l(t)} - \frac{(w_{11} - w_{13})}{\alpha_l} \right] \end{aligned} \quad (53)$$

If the adaptive law for the translation width is designed as

$$\dot{\hat{\varepsilon}}_l(t) = \frac{s_l(t)(w_{11} - w_{13})}{\alpha_l} \quad (54)$$

And, due to the analysis from (45)-(48), the inequality $s_1(w_{11} - w_{13}) \geq 0$. It is obvious that if the s_2 is approximately equal to zero, the tracking error s_1 will converge to zero. Thus, the next step is to control the differential pressure error is as small as possible.

Step 2: Taking the time derivative of (41)

$$\begin{aligned}\dot{s}_2 &= \dot{x}_3 - \dot{x}_{3d} \\ &= \bar{K} + u\bar{H} + d_2(t) - \dot{x}_{3d}\end{aligned}\quad (55)$$

Choosing the control signal u_{eq} as the solution of $\dot{s}_2(t) = 0$ without considering the uncertainty $d_2(t)$

$$u_{eq} = \bar{H}^{-1}(-\bar{K} + \dot{x}_{3d} - \Pi_2 s_2 - \bar{B}s_1)\quad (56)$$

where Π_2 is an arbitrary positive constant. As the outer loop, the optimal translation width, ε_2^* , which is obtained in (57) will be added to the control signal u by the similar fuzzy logic engine. Another adaptive law also derived in the sense of the Lyapunov stability theorem in order to turn the value of the translation width ε_2^* to confront with the system uncertainties online, and its estimated error can be defined as (58)

$$\varepsilon_2^* = \frac{|d_2|}{|w_{21} - w_{23}|\bar{H}} + \gamma_2\quad (57)$$

$$\tilde{\varepsilon}_2(t) = \hat{\varepsilon}_2(t) - \varepsilon_2^*\quad (58)$$

Let the sliding surface s_2 be the input linguistic variable of the fuzzy logic, which is the same as the outer loop, and let the control signal u be the output linguistic variable. The triangular membership functions and center average defuzzification method are also adopted in the inner loop, and the membership function is shown in Figure 17. Thus, the control signal is obtained as

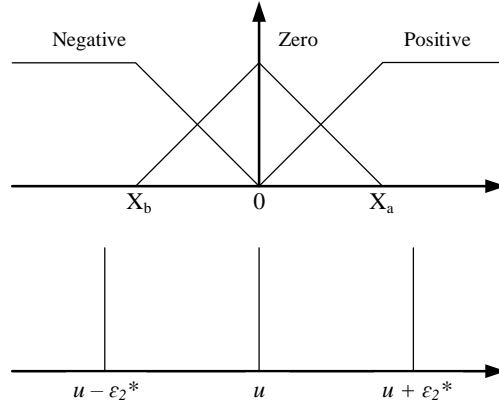


Figure 17 Membership functions of fuzzy sets for EFSMC of inner loop

$$\hat{u} = u_{eq} - \hat{\varepsilon}_2 (w_{21} - w_{23}) \quad (59)$$

Consider the Lyapunov function for the inner loop with the small positive constant α_2 as

$$V = V_1 + \frac{s_2^2(t) + \alpha_2 \tilde{\varepsilon}_2(t)}{2} \quad (60)$$

The Lyapunov derivative is as follows:

$$\begin{aligned} \dot{V} &= \dot{V}_1 + s_2 \dot{s}_2 + \alpha_2 \tilde{\varepsilon}_2 \dot{\tilde{\varepsilon}}_2 \\ &= \bar{B}s_1 s_2 - \Pi_1 s_1^2 - s_1(t) \gamma_1 (w_{11} - w_{13}) + \alpha_2 \tilde{\varepsilon}_2(t) \dot{\tilde{\varepsilon}}_2(t) - s_2(t) [\Pi_2 s_2 + \bar{B}s_1 + \bar{H} \hat{\varepsilon}_2(t) (w_{21} - w_{23}) - d_2(t)] \\ &= -\Pi_1 s_1^2 - \Pi_2 s_2^2 - s_1(t) \gamma_1 (w_{11} - w_{13}) + \alpha_2 \tilde{\varepsilon}_2(t) \dot{\tilde{\varepsilon}}_2(t) - \bar{H} s_2(t) \left[\varepsilon_2^* (w_{21} - w_{23}) - \frac{d_2(t)}{\bar{H}} + \hat{\varepsilon}_2(t) (w_{21} - w_{23}) - \varepsilon_2^* (w_{21} - w_{23}) \right] \\ &= -\Pi_1 s_1^2 - \Pi_2 s_2^2 - s_1(t) \gamma_1 (w_{11} - w_{13}) - \bar{H} s_2(t) (w_{21} - w_{23}) \left[\frac{|d_2(t)|}{\bar{H} |w_{21} - w_{23}|} + \gamma_2 - \frac{d_2(t)}{\bar{H} (w_{21} - w_{23})} \right] \\ &\quad - s_2(t) (w_{21} - w_{23}) \tilde{\varepsilon}_2(t) + \alpha_2 \tilde{\varepsilon}_2(t) \dot{\tilde{\varepsilon}}_2(t) \\ &\leq -\Pi_1 s_1^2 - \Pi_2 s_2^2 - s_1(t) \gamma_1 (w_{11} - w_{13}) - s_2(t) \gamma_2 \bar{H} (w_{21} - w_{23}) + s_2(t) \tilde{\varepsilon}_2(t) \alpha_2 \left[\frac{\dot{\tilde{\varepsilon}}_2(t)}{s_2(t)} - \frac{(w_{21} - w_{23})}{\alpha_2} \right] \end{aligned} \quad (61)$$

If the adaptive law for the inner loop is designed as

$$\dot{\tilde{\varepsilon}}_2(t) = \frac{s_2(t) (w_{21} - w_{23})}{\alpha_2} \quad (62)$$

Then (61) becomes

$$\dot{V} \leq -\Pi_1 s_1^2 - \Pi_2 s_2^2 - s_1(t) \gamma_1 (w_{11} - w_{13}) - s_2(t) \gamma_2 \bar{H} (w_{21} - w_{23}) \quad (63)$$

According to the inequality $s_2 (w_{21} - w_{23}) \geq 0$ and the positive function \bar{H} , we can obtain $\dot{V}(t) \leq 0$, $\dot{V}(t)$ is negative semidefinite, which means that $V(t) \leq V(0)$. It implies that $s_1(t)$, $s_2(t)$, $\tilde{\varepsilon}_1(t)$, and $\tilde{\varepsilon}_2(t)$ are bounded. Therefore, the proposed controller satisfies the condition $\dot{V}(t) \leq 0$ or the closed-loop system is stable and $\lim_{t \rightarrow \infty} e = 0$ [38].

To make a comparison of the trajectory tracking performance and the robustness of the proposed controller, another backstepping proportional integral derivative (BPID) control and backstepping sliding mode control (BSMC) were also designed and embedded. The BPID shown in Figure 18 uses PD for the position control loop to realize the desired torque and PI in the inner loop for torque control. The control signal which is sent to the servo valve to control the manipulator can be expressed in the time domain as follows:

$$\tau_d(t) = K_{p1} e_p(t) + K_{D1} \frac{de_p(t)}{dt} \quad (64)$$

$$u(t) = K_{p2} e_t(t) + K_{I2} \int_0^t e_t(t) dt \quad (65)$$

where $e_p(t)$ is the position error between the desired angle set point and the output, $de_p(t)$ is the derivation of position error, $\tau_d(t)$ is the desired torque, K_{p1} is the proportional gain of outer loop, K_{D1} is the derivative gain. In the second PI controller, $e_t(t)$ is the error between the desired torque and the feedback, K_{p2} is the proportional gain of inner loop, K_{I2} is the integral gain, $u(t)$ is the control signal. These parameters are changed within their boundaries which are determined from practical experiments.

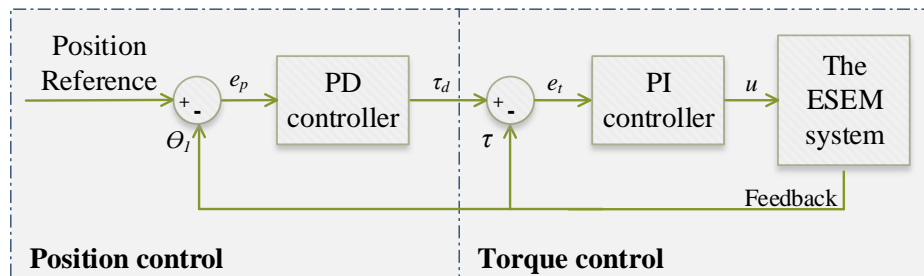


Figure 18 Scheme of BPID controller for the ESEM system

The BSMC uses two conventional SMC systems for two loops which has structure as Figure 19. Similarly to the proposed controller, the two sliding surfaces and their derivative are assigned as (39), (40), (41) and (55). The virtual torque $\tau_d(t)$ can be obtained as

$$\tau_d = \bar{B}^{-1} (\dot{x}_{2d} - c_1 \dot{e}_1 - \Gamma_1 s_1 - \bar{F} + \eta_1 \text{sign}(s_1)) \quad (66)$$

where Γ_1 is an arbitrary positive constant, the sign function $\text{sign}(s_1)$ is defined in (67)

$$\text{sign}(s_1) = \begin{cases} 1 & \text{if } s_1(t) \geq 0, \\ -1 & \text{if } s_1(t) < 0. \end{cases} \quad (67)$$

η_1 is the robust gain and to guarantee the stability of system based on Lyapunov theory, η_1 should be chosen as the boundary of the perturbation $d_1(t)$, $\eta_1 \geq \|d_1(t)\|_\infty$.

The control signal which is generated by the second SMC is

$$u = \bar{H}^{-1} (-\bar{K} + \dot{x}_{3d} - \Gamma_2 s_2 - \bar{B}s_1 + \eta_2 \text{sign}(s_2)) \quad (68)$$

where Γ_2 is an arbitrary positive constant, the sign function $\text{sign}(s_2)$ is defined in (69)

$$\text{sign}(s_2) = \begin{cases} 1 & \text{if } s_2(t) \geq 0, \\ -1 & \text{if } s_2(t) < 0. \end{cases} \quad (69)$$

η_2 is the robust gain and to guarantee the stability of system based on Lyapunov theory, η_2 should be chosen as the boundary of the hydraulic perturbation $d_2(t)$, $\eta_2 \geq \|d_2(t)\|_\infty$.

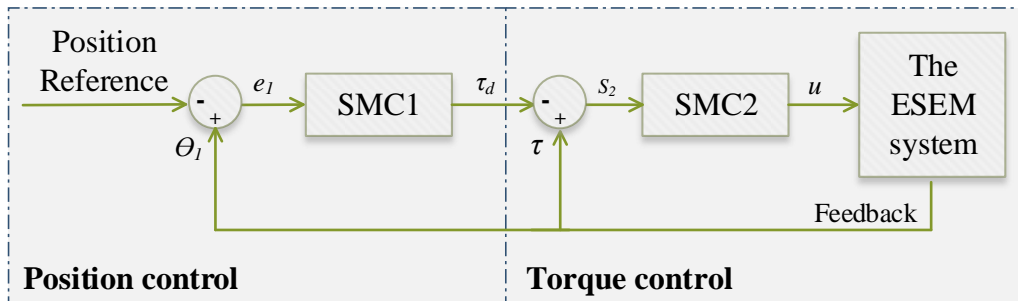


Figure 19 Scheme of BSMC controller for the ESEM system

EXPERIMENTAL RESULTS

4.1 Test bench setup

Figure 20 shows the schematic diagram of the proposed ESEM. The system hardware includes three main parts, named the hydraulic subsystem, the mechanical subsystem, and the VSA system. Two encoders are used to measure the rotational motion of the two links. A loadcell (YM13 – 100K) connecting the cylinder and the flexible joint is used to identify torques acting on the rod. The pressure in two chambers is obtained by two pressure sensors. In Figure 8, another encoder mounted to the DC motor to feedback the position of the nut. The setting parameters for the ESEM system are as shown in Table 4.

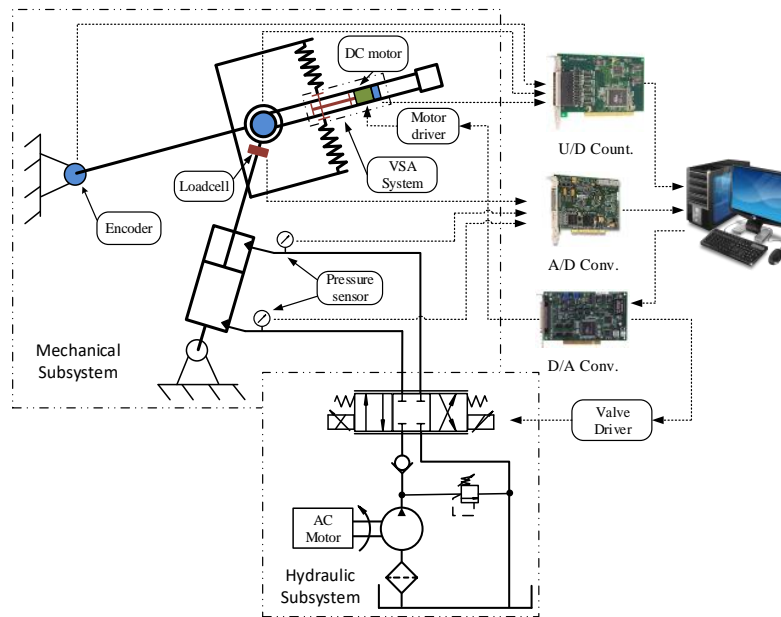


Figure 20 Schematic diagram of the electrohydraulic-series-elastic-manipulator system

Table 4 Setting parameters for the ESEM system

Components	Parameters	Specification
Hydraulic Pump	Displacement	3.6 [cc/rev]
	Rated rotation speed	1730 [rpm]

	Relief pressure	150 [bar]
Servo valve	Model	MOOG – D633
	Rated flow	10 [l/min]
Hydraulic Cylinder	Tube diameter – D	46 [mm]
	Rod diameter – d	22 [mm]
	Length of stroke – l_{cyl}	35 [mm]
Hydraulic oil	Effective bulk modulus	1.5×10^9 [Pa]
	Specific gravity	0.87
Load cell	Capacity	100 [kgf]
	Rated Output	2.052 [mV/V]
Encoder	Model	E60H
	Resolution	8192 [p/rev]
Pressure Sensor	Capacity	160 [bar]
	Rated Output	16 [bar/V]
DC Motor	Model	IG – 36PGM
	Gear Head Reduction Ratio	1/5
	Encoder resolution	26 [p/rev]

The proposed controller is implemented on an Advantech Industrial computer (Core i5 3.5 GHz) within Simulink environment combined and Real-time Windows Target Toolbox of MATLAB. An encoder Quad-04 card from Measure Computing Corporation uses to collect data of three encoders and two multifunction data acquisition Advantech cards, A/D 1711 and A/D 6220, are installed in the PCI slots of the PC to perform the peripheral interfaces. The experimental apparatus is shown in Figure 21.

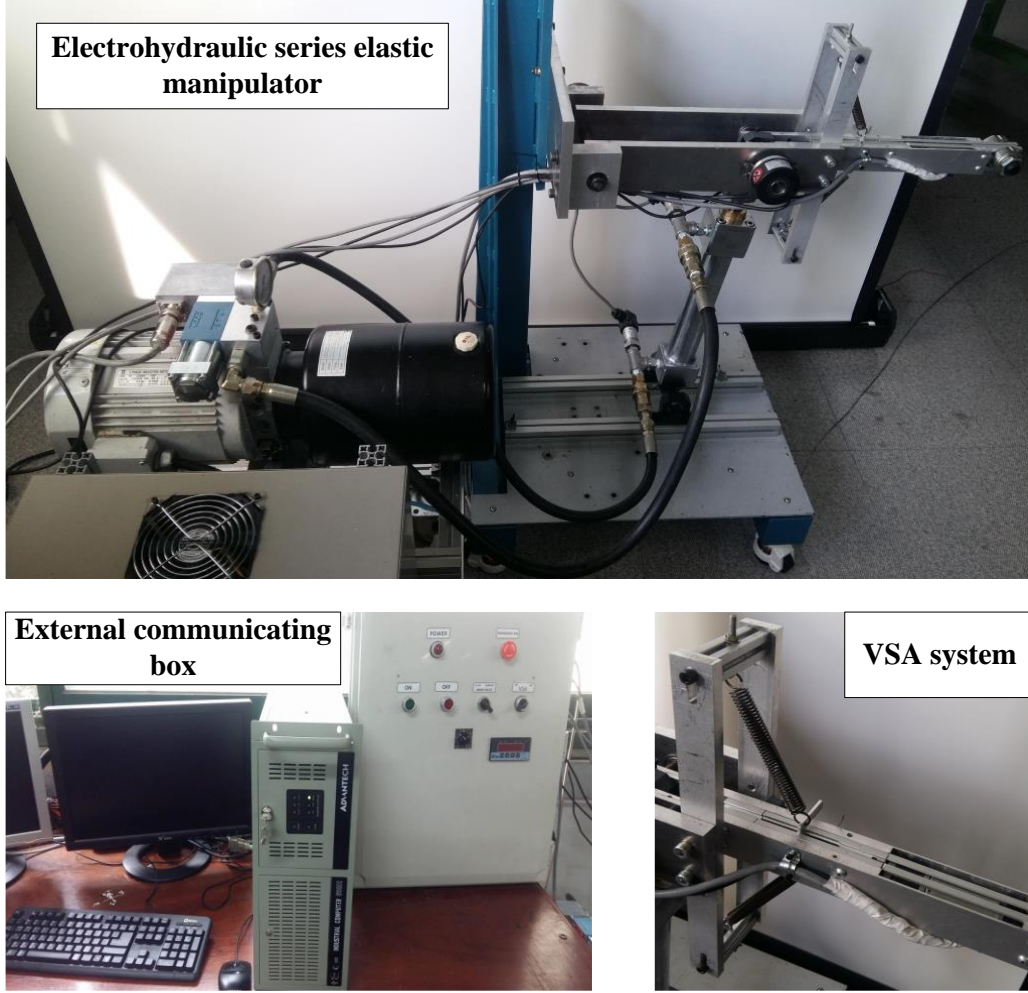


Figure 21 The experimental apparatus

In this section, a number of experiments were carried out to prove the effectiveness of the proposed controller. The control algorithms were built by the combination of Simulink and the Real-time Windows Target Toolbox of MATLAB. The VSA system was adjusted to lowest stiffness, $x_{vsa}=0$, at the first ten seconds, to highest stiffness, $x_{vsa}=50$, at the last ten seconds in case 2, case 3, and to random positions in case 4. The system parameters were adopted carefully based on the model design and experimental processes. All the parameters of the above controllers are chosen to achieve the best transient control performance as follows

- BPID: $K_{p1} = 1.1 \times 10^6$, $K_{I1} = 0$, $K_{D1} = 2 \times 10^3$, $K_{p2} = 2 \times 10^{-3}$, $K_{I2} = 7$, $K_{D2} = 0$.
- BSMC: $c_1 = 60$, $\Gamma_1 = 850$, $\eta_1 = 1$, $\Gamma_2 = 6.72 \times 10^{10}$, $\eta_2 = 6 \times 10^8$.
- BAEFSMC: $c_1 = 60$, $\Pi_1 = 900$, $\alpha_1 = 0.01$, $\Pi_2 = 6.72 \times 10^{10}$, $\alpha_2 = 0.5$.

4.2 The variation performance of the VSA system

First of all, to investigate the dynamic characteristic of the proposed VSA system, an experiment was setup using a PID controller with $K_{PI} = 2.5$, $K_{II} = 0.4$, $K_{DI} = 0.05$. The responses of the VSA to sinusoidal $y = 10 \sin(\omega_o t)$ at the nut's starting position of 25 mm with ω_o from 0.1 to 7 rad/sec in the frequency domain were collected to plot the Bode diagram shown in Figure 22. The PID controller shows the ability of closely tracking to the input signals that are lower than 3 rad/sec. The bandwidth of the proposed VSA in this case is about 5.8 rad/sec. This PID controller will be used to control the position of the ball screws nut, x_{vsa} , for next case studies.

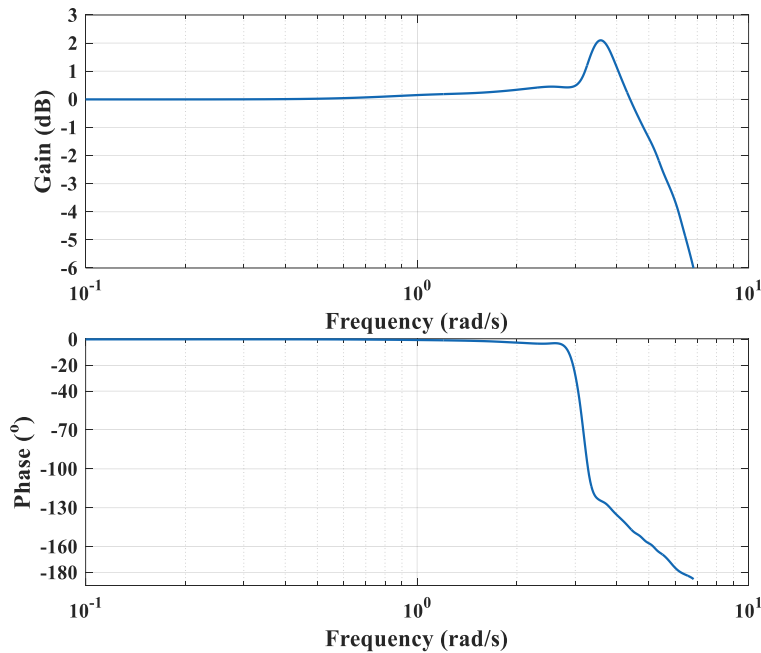


Figure 22 Bode plot of the VSA system with a PID controller

4.3 Case study 1

In this case, the ESEM tracks to the desired trajectory as a sinusoidal $r(t) = 12 + 10 \sin(2\pi t)$, the comparison of position and torque response, control signal is presented in Figure 23 to Figure 25. From the results, we can realize that the BPID controller provides a worst response. Due to the presence of nonlinearities and uncertainties, the BPID controller cannot ensure accurate trajectory tracking. The proposed controller performs a favorable tracking response not only at position control loop but also at torque control loop. A little vibration occurs at cylinder's starting point but the ESEM quickly tracks to the reference with steady state error in a range of $[-0.02 \ 0.03]$ degree. The control

signal in comparison with BSMC shows that the chattering phenomenon is reduced significantly according to the online adjustment of the translation width.

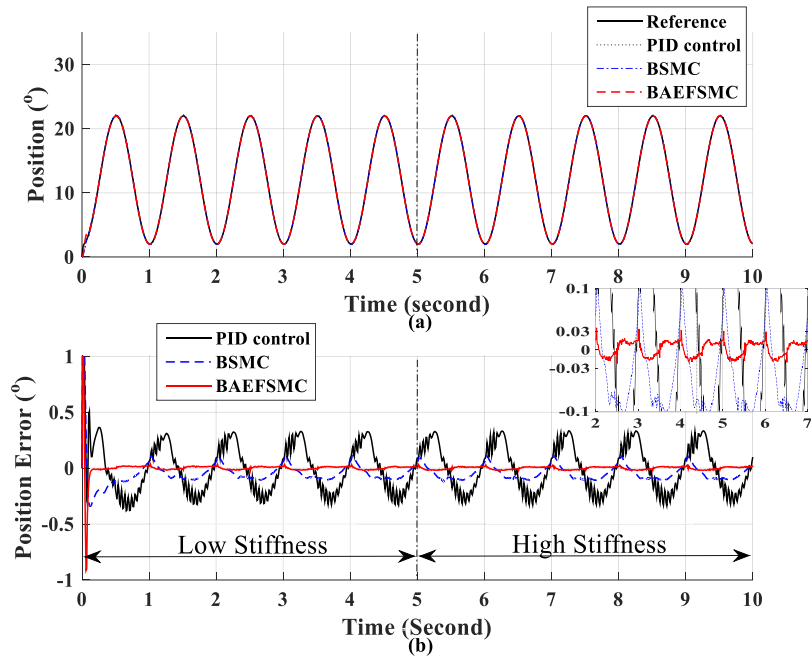


Figure 23 Comparison of the sinusoidal response of the ESEM system.

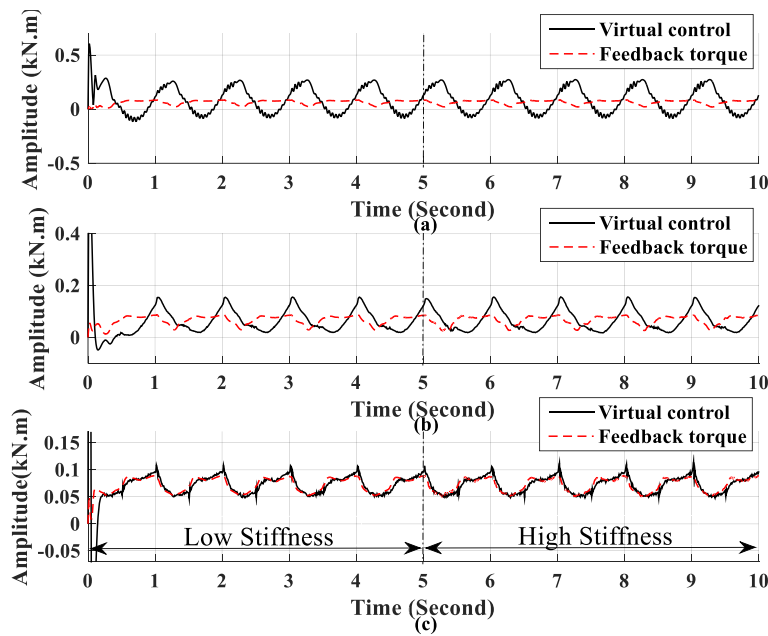


Figure 24 Comparison of the sinusoidal torque response of the ESEM system. a) PID b) BSMC c) BAEFSMC

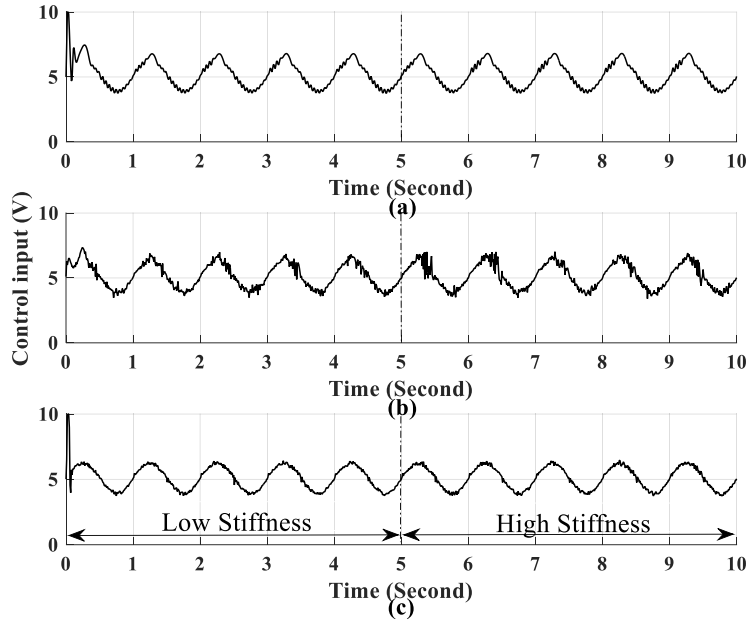


Figure 25 Comparison of the sinusoidal control signal. a) PID b) BSMC c) BAEFSMC

4.4 Case study 2

Since the ESEM is a low-bandwidth system, and to enable the capability of suppressing vibration of the IS, the reference signal must go through an appropriate low-pass filter. For the first case study, the performance of these controllers to the pulse trajectory tracking is shown in Figure 26, Figure 27 and Figure 28. The response shows that using the proposed controller, the ESEM system performs a better convergence and more stable in both position and torque control loop. The first link reaches to the desired position much faster than the other, and the steady state error is bounded in a range of $[-0.02 \ 0.02]$. In the inner loop, the virtual torque is generated very close to the feedback torque. The chattering phenomenon also reduces significantly compared to the BSMC.

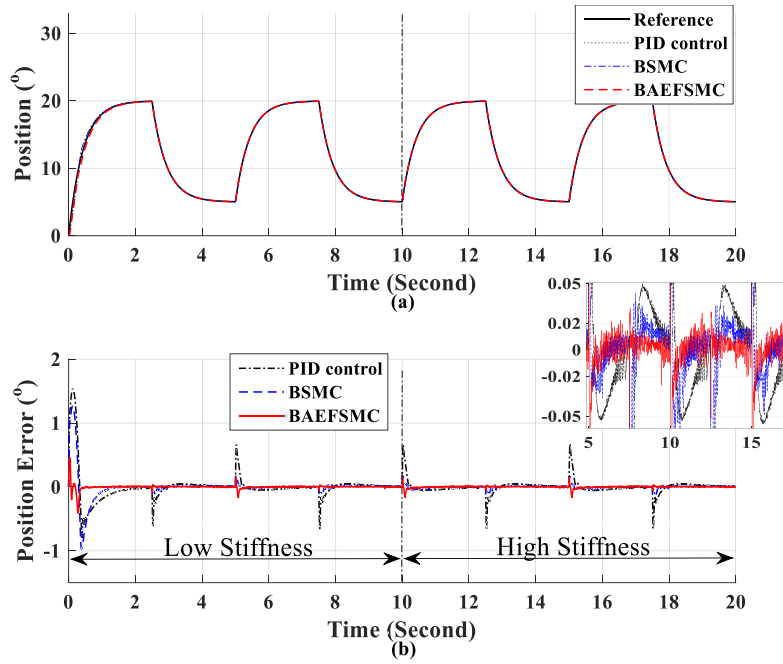


Figure 26 Comparison of the pulse position response of the ESEM system.

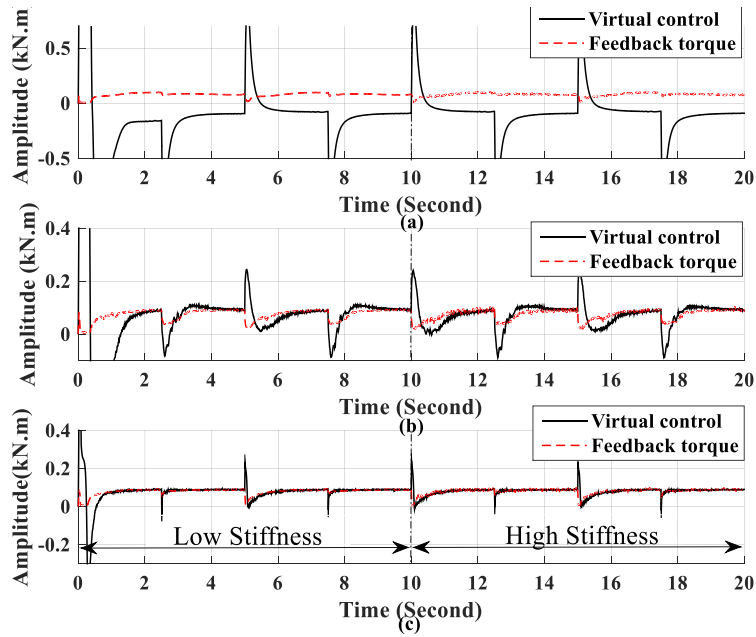


Figure 27 Comparison of the pulse torque response of the ESEM system. a) PID b) BSMC c) BAEFSMC

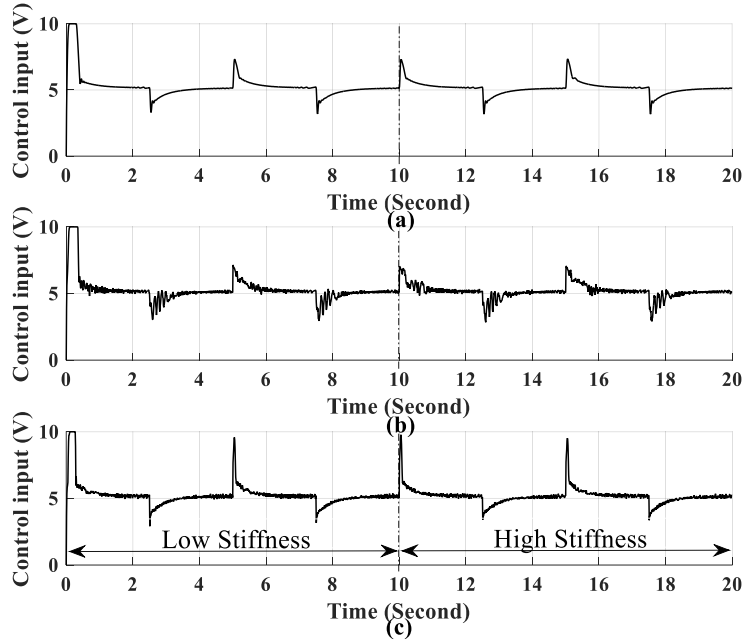


Figure 28 Comparison of the pulse control signal. a) PID b) BSMC c) BAEFSMC

4.5 Case study 3

This case study discusses the tracking task of multi-step trajectory. The responses of the ESEM system with these controllers, system states, control signals are shown in Figure 29, Figure 30 and Figure 31, respectively. As shown in these figures, the ABEFSMC is able to maintain excellent performance even with the large range of setpoint and high stiffness working condition. The steady error is still bounded in the range of $[-0.02 \ 0.02]$. The feedback torque keeps tracking to the virtual torque control effort in Figure 30c which means that all defined states are stable. Therefore, the robust tracking performance is guaranteed by the presence of parameter variations and external load disturbance. The translation widths in both loops also play a good role in reducing the chattering phenomenon.

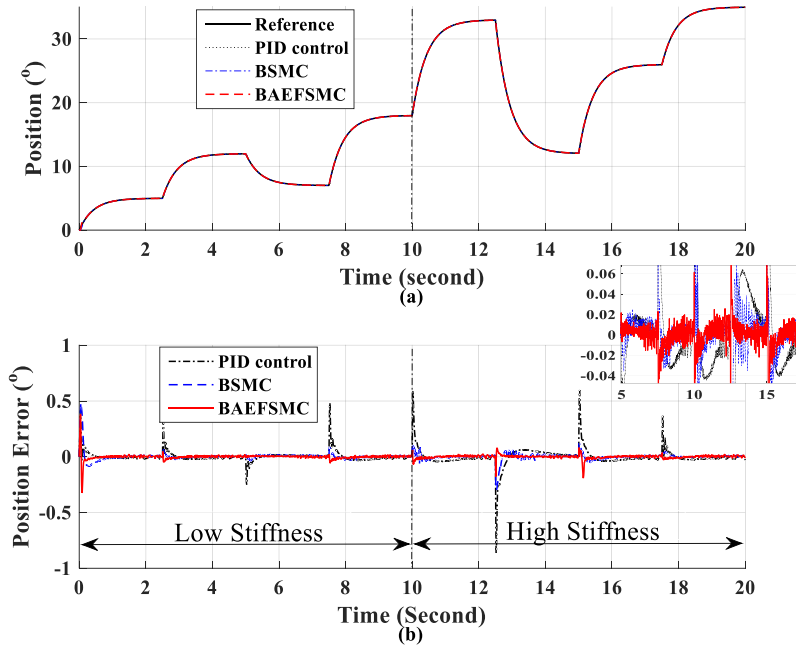


Figure 29 Comparison of the multi-step position response of the ESEM system.

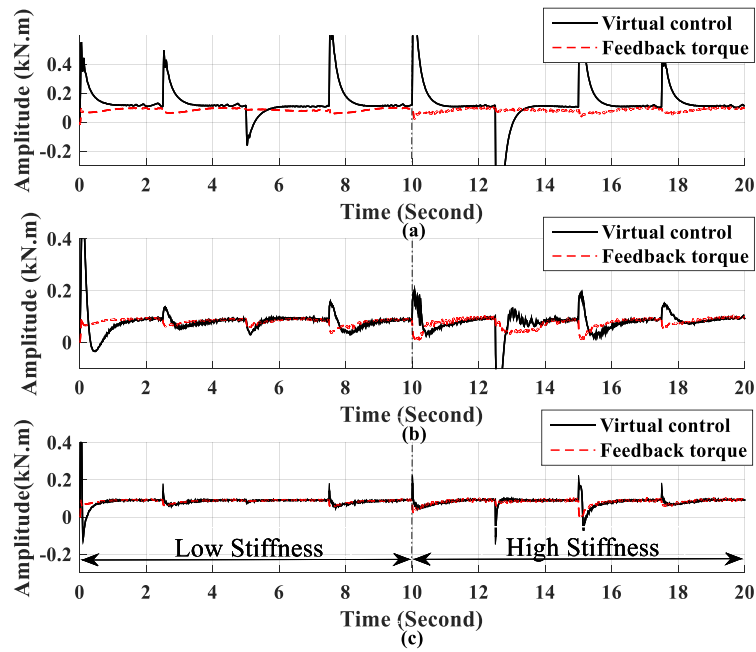


Figure 30 Comparison of the multi-step torque response of the ESEM system. a) PID b) BSMC c) BAEFSMC

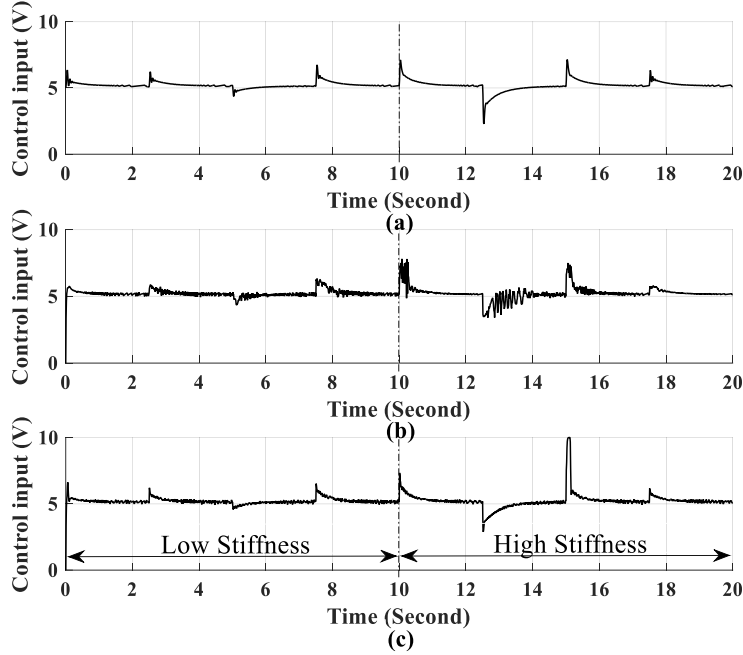


Figure 31 Comparison of the multi-step control signal. a) PID b) BSMC c) BAEFSMC

4.6 Case study 4

In the fourth case study, the effectiveness of the hybrid controller, especially the FIS, in vibration control for the repetitive task is presented. As the result of the second case study, the response of the second link to the pulse trajectory with the BAEFSMC at the lowest stiffness working condition, $x_{vsa} = 0$, was used to calculate the parameters of the ZV and the ZVD. The oscillation of the end effector was translated into a peak in the periodogram as shown in Figure 32. According to the result, the estimated value of the natural frequency is 4.93 Hz. In the other hand, the damping ratio was obtained by [37] is 0.037. By using these values, another experiment was setup to illustrate the influence of the changing stiffness to the IS performance. The ESEM tracked to the shaped and unshaped pulse trajectory while the VSA position keeps increasing to the random values. The response of the end effector corresponding to each position is shown in Figure 33 and Figure 34. The black dotted line is the vibration of the end effector without using the IS, and the blue line are the vibration of the end effector with the ZV and the ZVD. It is obvious that the VSA position is at 0, the ZV and ZVD suppress the vibration excellently due to the small error in the estimated values. The more the VSA position increases the larger amplitude of the residual vibration gets. Although the ZVD is more robust than the ZV [8], it cannot perform well in such a large range of stiffness varying. Besides the effect of gravity also causes the different oscillation in both directions of the cylinder.

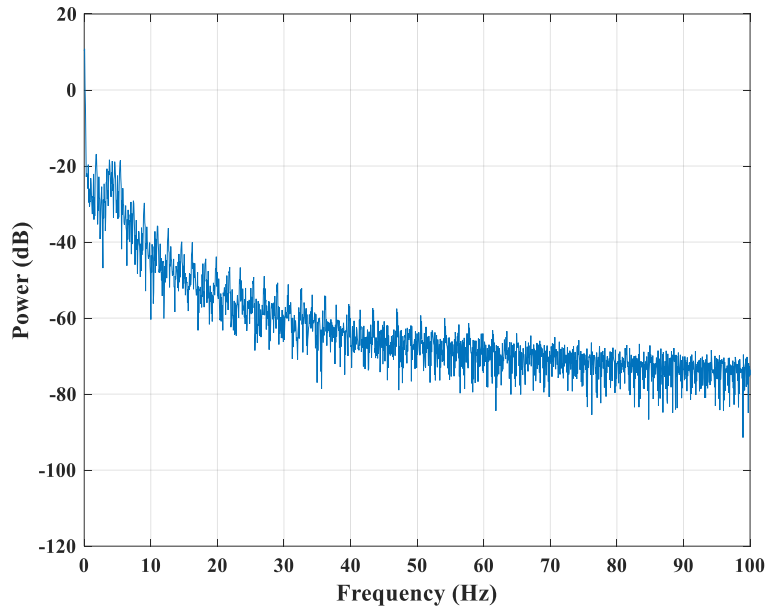


Figure 32 The periodogram of the end effector oscillation

To overcome the problems mentioned above, the fuzzy logic engine designed in section 3 was used to update the ZV parameters online corresponding to the VSA position and the cylinder actions. As the results presented in Figure 35, the vibration is vanished stably against the stiffness adjusting. The ZV parameters quickly change to the optimal values so that the vibration suppression will not be affected by the parameters turning. The FIS fuzzy output gain is shown in Figure 36. The comparison of vibration response at two positions, $x_{vsa} = 37$ and $x_{vsa} = 45$, is zoomed in Figure 37. The presence of the FIS does not cause any influence on the precise trajectory tracking of the ESEM system. The position response of the manipulator using BAEFSMC with FIS is displayed in Figure 38. The associated tracking error still remains in $[-0.02 \ 0.02]$.

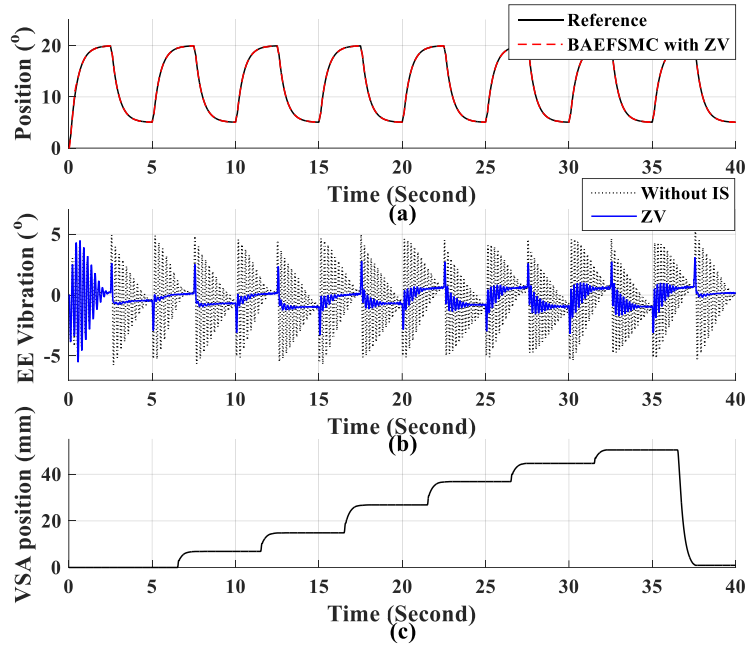


Figure 33 Vibration response of the end effector with ZV

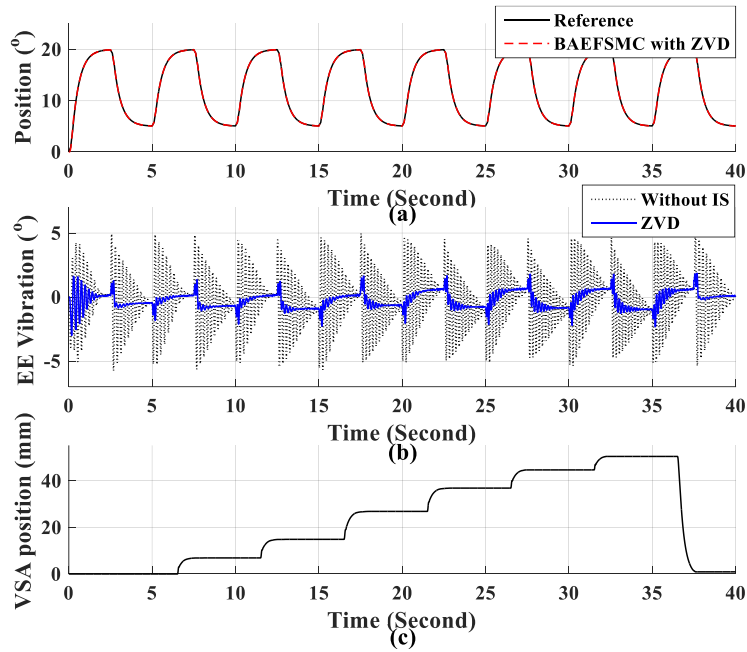


Figure 34 Vibration response of the end effector with ZVD

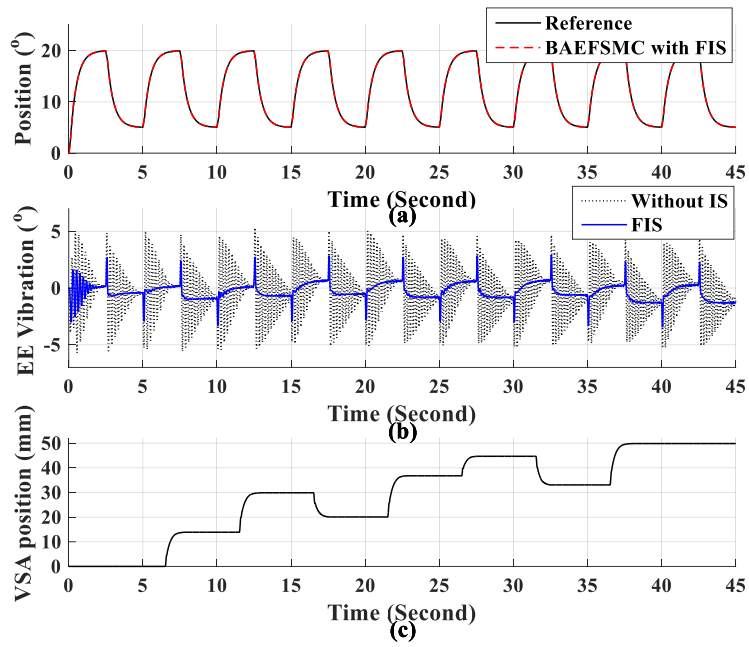


Figure 35 The vibration response of the end effector with FIS

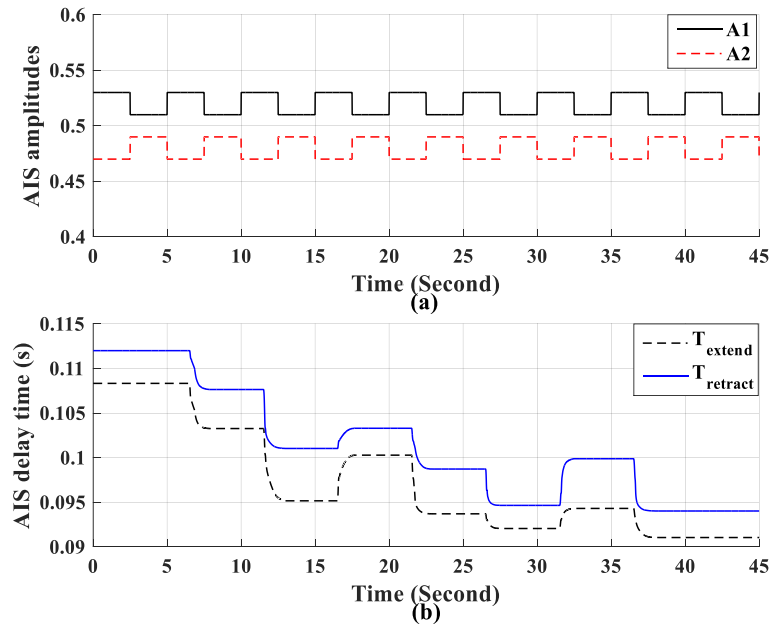


Figure 36 The adaptive parameters of the FIS

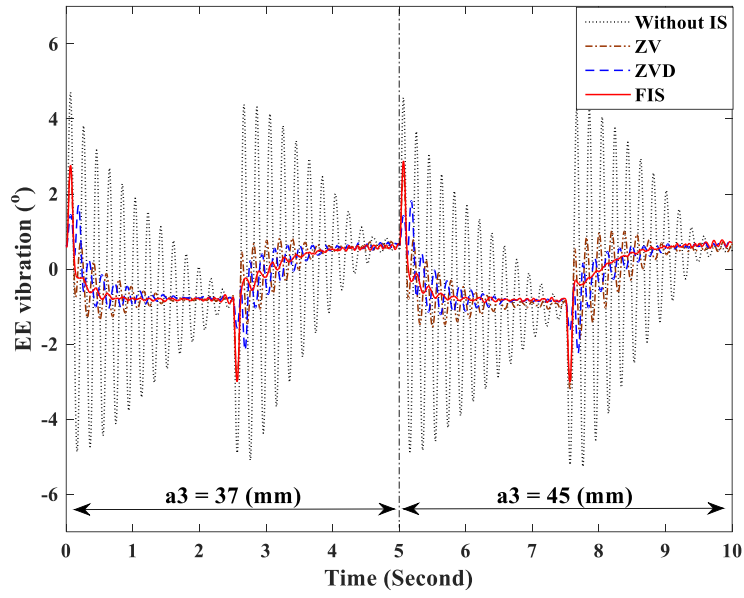


Figure 37 The vibration response at two positions of the VSA

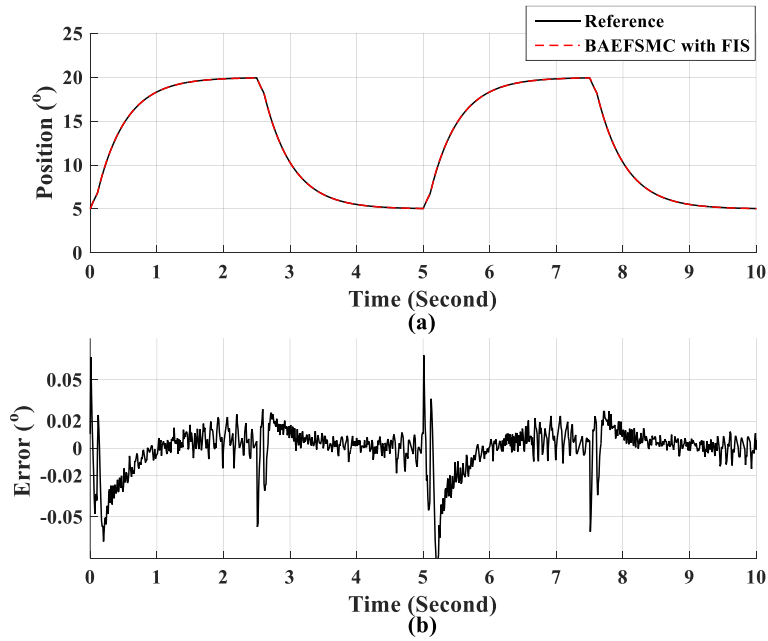


Figure 38 Position response of the ESEM system with BAEFSMC and FIS

CONCLUSIONS AND FUTURE WORKS

This study proposed and investigated an electrohydraulic series elastic manipulator containing a novel variable stiffness actuator. Some key problems were discussed and solved such as how to provide precise trajectory tracking control as well as suppress the residual vibration robustly to the variable adjustment.

Chapter 2 analyzed and expounded the proposed system. The novel variable stiffness actuator is able to provide an ability of wide variety of joint stiffness, high dynamic due to the independent operating of primary torque generator. The bandwidth of the VSA system could be up to 5.8 rad/sec. All hydraulic components, the two-link robotic manipulator and the variable stiffness actuator were mathematically modeled based on parameters of the testbench. An advanced approach was used to include the hydraulic actuator dynamic in other to reduce the influence of the nonlinear characteristics of the hydraulic subsystem as well as the derivative action in the conventional backstepping technique.

For the position and vibration control purpose, the VSA used two soft springs and acting as a disturbance source. Since this system is a complex high order and highly nonlinear system, two adaptive enhanced fuzzy sliding mode control systems were designed in chapter 3 for two system states by using backstepping technique to reduce the order of model and guarantee the stability and the robustness of the whole plant in the presence of nonlinear elements and disturbances. A translation width was applied to two loops to remedy the chattering phenomenon. The adaptive laws were derived from the sense of Lyapunov stability theorem to update the value of translation width online. A fuzzy engine was designed and embedded in the vibration control loop to keep the robustness of the ZV by turning the ZV parameters according to ball screws nut position and the cylinder action. Experiments were carried out to evaluate the effectiveness of the proposed controller. The results show that the hybrid controller was successfully employed and achieved a good performance at both position and vibration control.

The hydraulic dynamics is mainly affected by the parametric uncertainties such as temperature, Bulk modulus, friction, *etc.* In other to increase the precision position control and the robustness of the controller, additional adaptive parameter rules should be added to the proposed controller in future work. Moreover, the fuzzy input shaping was

used in this study only considering the fixed load at the end effector. For variety load condition, the FIS needs to utilize additional observer to feedback further information for the FIS.

Reference

- [1] S. A. Migliore, E. A. Brown, and S. P. DeWeerth, "Novel Nonlinear Elastic Actuators for Passively Controlling Robotic Joint Compliance," *Journal of Mechanical Design*, vol. 129, pp. 406-412, 2006.
- [2] N. G. T. Bram Vanderborght, Claudio Semini, Ronald Van Ham, Darwin G. Caldwell, "MACCEPA 2.0: Adjustable Compliant Actuator with Stiffening Characteristic for Energy Efficient Hopping."
- [3] A. Jafari, N. G. Tsagarakis, I. Sardellitti, and D. G. Caldwell, "A New Actuator With Adjustable Stiffness Based on a Variable Ratio Lever Mechanism," *IEEE/ASME Transactions on Mechatronics*, vol. 19, pp. 55-63, 2014.
- [4] A. Jafari, N. G. Tsagarakis, and D. G. Caldwell, "A Novel Intrinsically Energy Efficient Actuator With Adjustable Stiffness (AwAS)," *IEEE/ASME Transactions on Mechatronics*, vol. 18, pp. 355-365, 2013.
- [5] S. S. Groothuis, G. Rusticelli, A. Zucchelli, S. Stramigioli, and R. Carloni, "The Variable Stiffness Actuator vsaUT-II: Mechanical Design, Modeling, and Identification," *IEEE/ASME Transactions on Mechatronics*, vol. 19, pp. 589-597, 2014.
- [6] W. Wang, X. Fu, Y. Li, and C. Yun, "Design of Variable Stiffness Actuator Based on Modified Gear–Rack Mechanism," *Journal of Mechanisms and Robotics*, vol. 8, pp. 061008-061008-10, 2016.
- [7] G. Tonietti, R. Schiavi, and A. Bicchi, "Design and Control of a Variable Stiffness Actuator for Safe and Fast Physical Human/Robot Interaction," in *Proceedings of the 2005 IEEE International Conference on Robotics and Automation*, 2005, pp. 526-531.
- [8] N. C. Singer and W. P. Seering, "Preshaping Command Inputs to Reduce System Vibration," *Journal of Dynamic Systems, Measurement, and Control*, vol. 112, pp. 76-82, 1990.
- [9] M. Z. M. Zain, M. O. Tokhi, and Z. Mohamed, "Hybrid learning control schemes with input shaping of a flexible manipulator system," *Mechatronics*, vol. 16, pp. 209-219, 2006/04/01/ 2006.
- [10] M. Agostini, G. G. Parker, K. Groom, H. Schaub, and R. D. Robinett, "Command shaping and closed-loop control interactions for a ship crane," in *Proceedings of the 2002 American Control Conference (IEEE Cat. No.CH37301)*, 2002, pp. 2298-2304 vol.3.
- [11] E. Pereira, J. R. Trapero, I. M. Díaz, and V. Feliu, "Adaptive input shaping for single-link flexible manipulators using an algebraic identification," *Control Engineering Practice*, vol. 20, pp. 138-147, 2012/02/01/ 2012.

- [12] P. Juyi, C. Pyung-Hun, P. Hyung-Soon, and L. Eunjeong, "Design of learning input shaping technique for residual vibration suppression in an industrial robot," *IEEE/ASME Transactions on Mechatronics*, vol. 11, pp. 55-65, 2006.
- [13] D. Q. Truong and K. K. Ahn, "Parallel control for electro-hydraulic load simulator using online self tuning fuzzy PID technique," *Asian Journal of Control*, vol. 13, pp. 522-541, 2011.
- [14] D. Q. Truong and K. K. Ahn, "Force control for hydraulic load simulator using self-tuning grey predictor – fuzzy PID," *Mechatronics*, vol. 19, pp. 233-246, 2009/03/01/ 2009.
- [15] D. Q. Truong and K. K. Ahn, "Force control for press machines using an online smart tuning fuzzy PID based on a robust extended Kalman filter," *Expert Systems with Applications*, vol. 38, pp. 5879-5894, 2011/05/01/ 2011.
- [16] L. D. Re and A. Isidori, "Performance enhancement of nonlinear drives by feedback linearization of linear-bilinear cascade models," *IEEE Transactions on Control Systems Technology*, vol. 3, pp. 299-308, 1995.
- [17] Y. Liu and H. Handroos, "Technical note Sliding mode control for a class of hydraulic position servo," *Mechatronics*, vol. 9, pp. 111-123, 1999/02/01/ 1999.
- [18] M.-c. Wu and M.-c. Shih, "Simulated and experimental study of hydraulic anti-lock braking system using sliding-mode PWM control," *Mechatronics*, vol. 13, pp. 331-351, 2003/05/01/ 2003.
- [19] B. Bandyopadhyay, S. Janardhanan, and S. K. Spurgeon, *Advances in Sliding Mode Control: Concept, Theory and Implementation*. Berlin, Germany: Springer-Verlag, 2013.
- [20] T. H. Ho and K. K. Ahn, "Speed Control of a Hydraulic Pressure Coupling Drive Using an Adaptive Fuzzy Sliding-Mode Control," *IEEE/ASME Transactions on Mechatronics*, vol. 17, pp. 976-986, 2012.
- [21] K. K. Ahn, D. N. C. Nam, and M. Jin, "Adaptive Backstepping Control of an Electrohydraulic Actuator," *IEEE/ASME Transactions on Mechatronics*, vol. 19, pp. 987-995, 2014.
- [22] D. Garagic and K. Srinivasan, "Application of nonlinear adaptive control techniques to an electrohydraulic velocity servomechanism," *IEEE Transactions on Control Systems Technology*, vol. 12, pp. 303-314, 2004.
- [23] S. Haddadin, R. Belder, and A. Albu-Schäffer, "Dynamic Motion Planning for Robots in Partially Unknown Environments*," *IFAC Proceedings Volumes*, vol. 44, pp. 6842-6850, 2011/01/01/ 2011.
- [24] S. Haddadin, M. Weis, S. Wolf, and A. Albu-Schäffer, "Optimal Control for Maximizing Link Velocity of Robotic Variable Stiffness Joints," *IFAC Proceedings Volumes*, vol. 44, pp. 6863-6871, 2011/01/01/ 2011.

- [25] H. Schempf, C. Kraeuter, and M. Blackwell, "Roboleg: a robotic soccer-ball kicking leg," in *Proceedings of 1995 IEEE International Conference on Robotics and Automation*, 1995, pp. 1314-1318 vol.2.
- [26] M. Garabini, A. Passaglia, F. Belo, P. Salaris, and A. Bicchi, "Optimality principles in variable stiffness control: The VSA hammer," in *2011 IEEE/RSJ International Conference on Intelligent Robots and Systems*, 2011, pp. 3770-3775.
- [27] M. Krstic, I. Kanellakopoulos, and P. V. Kokotovic, *Nonlinear and Adaptive Control Design*. New York, USA, 1995.
- [28] W. Rong-Jong and S. Kuo-Ho, "Adaptive enhanced fuzzy sliding-mode control for electrical servo drive," *IEEE Transactions on Industrial Electronics*, vol. 53, pp. 569-580, 2006.
- [29] K. F. Laurin-Kovitz, J. E. Colgate, and S. D. R. Carnes, "Design of components for programmable passive impedance," in *Proceedings. 1991 IEEE International Conference on Robotics and Automation*, 1991, pp. 1476-1481 vol.2.
- [30] C. Ching-Ping and B. Hannaford, "Measurement and modeling of McKibben pneumatic artificial muscles," *IEEE Transactions on Robotics and Automation*, vol. 12, pp. 90-102, 1996.
- [31] E. P. B. Siciliano and P. O. Khatib, *Springer Handbook of Robotics*. Springer Berlin Heidelberg, 2008.
- [32] G. Hirzinger, N. Sporer, A. Albu-Schaffer, M. Hahnle, R. Krenn, A. Pascucci, *et al.*, "DLR's torque-controlled light weight robot III-are we reaching the technological limits now?," in *Proceedings 2002 IEEE International Conference on Robotics and Automation (Cat. No.02CH37292)*, 2002, pp. 1710-1716 vol.2.
- [33] N. Niksefat and N. Sepehri, "Designing robust force control of hydraulic actuators despite system and environmental uncertainties," *IEEE Control Systems*, vol. 21, pp. 66-77, 2001.
- [34] J. J. Craig, *Introduction to Robotics: Mechanics and Control*. Pearson/Prentice Hall, 2005.
- [35] R. L. Farrenkopf, "Optimal Open-Loop Maneuver Profiles for Flexible Spacecraft," *Journal of Guidance, Control, and Dynamics*, vol. 2, pp. 491-498, 1979/11/01 1979.
- [36] C. J. Swigert, "Shaped Torque Techniques," *Journal of Guidance, Control, and Dynamics*, vol. 3, pp. 460-467, 1980/09/01 1980.
- [37] L. Meirovitch, *Elements of Vibration Analysis*. McGraw-Hill, 1986.
- [38] J. J. E. Slontine and W. Li, *Applied Nonlinear Control*. NJ: Prentice-Hall, 1991.
- [39] L. X. Wang, *A Course in Fuzzy Systems and Control*. Englewood Cliffs, NJ: Prentice-Hall 1997.